FlatChem xxx (2017) xxx–xxx

Contents lists available at ScienceDirect

FlatChem

journal homepage: www.elsevier.com/locate/flatc

Self-organized growth and self-assembly of nanostructures on 2D materials

Jiwoong Yang [a,b], Kihwan Kim [c], Yangjin Lee [d], Kwanpyo Kim [d,*], Won Chul Lee [c,*], Jungwon Park [a,b,*]

[a] Center for Nanoparticle Research, Institute for Basic Science (IBS), Seoul 08826, Republic of Korea
[b] School of Chemical and Biological Engineering, Seoul National University, Seoul 08826, Republic of Korea
[c] Department of Mechanical Engineering, Hanyang University, Ansan, Gyeonggi 15588, Republic of Korea
[d] Department of Physics, Ulsan National Institute of Science and Technology (UNIST), Ulsan 44919, Republic of Korea

ARTICLE INFO

Article history:
Received 30 April 2017
Revised 11 July 2017
Accepted 12 July 2017
Available online xxxx

Keywords:
2D materials
Self-organized growth
Heterostructures
Self-alignment
Self-assembly

ABSTRACT

Two-dimensional (2D) composite materials have gained much interest, and their synthesis and characterization have been intensively investigated to fully exploit the new functionalities and realize their potential applications. Among the various approaches to prepare heterostructures based on 2D materials, the process of self-organization between different materials is widely employed to obtain a wide range of ordered heterostructures. In this review article, we introduce notable achievements in the domain of self-organized growth of nanostructures on 2D materials. Various examples and synthetic approaches for the self-organized growth of organic molecules, inorganic nanomaterials, and 2D materials, which result in the formation of different types of heterostructures, have been discussed. We especially focus on the self-aligned growth of nanostructures on 2D materials, governed by the van der Waals interaction between the grown nanostructures and 2D substrates. The assembly of various nanostructures on the 2D moiré periodic potential is also highlighted. Finally, we remark the representative applications of the self-organized growth behaviors such as advanced nanofabrication and the mapping of crystal domains of 2D materials.

© 2017 Elsevier B.V. All rights reserved.

Introduction

Two-dimensional (2D) materials, i.e., crystals with a single layer of atoms, have attracted widespread interest from researchers of various disciplines including chemistry, physics, materials science, and engineering because of their unique properties [1–3]. Since the emergence of graphene, 2D materials of metals, semiconductors, and insulators have been intensively studied to develop new synthetic pathways, examine physical properties, and find applications to utilize their unique properties. Because 2D materials are one atom-thick, the surfaces of the constituent atoms are entirely exposed. This hundred percent surface-to-volume ratio provides an opportunity to exploit the van der Waals interaction in assembling the nanostructures on 2D materials (Fig. 1). For this reason, heterostructures composed of nanomaterials and 2D materials are often called van der Waals heterostructures. One of the most important motivations for developing heterostructures based on 2D materials is that the resulting physical properties of the heterostructures can be extensively tuned due to the coupling of a large portion of surface atoms with the counter material. Furthermore, many of those physical properties are dependent on the relative crystallographic orientations of the constituent materials.

One of the well-known examples for the properties depending on stacking-orientation is the bilayer graphene, which is the simplest representative of van der Waals structure [4,5]. First, the electronic properties of graphene are highly dependent on the thickness of the graphene layers. Interestingly, in vertical electric fields, a band gap is induced in the Bernal-stacked (AB stacked) bilayer graphene [6], whereas two layers of monolayer graphene without Bernal stacking act as two individual monolayers [7]. More examples on heterostructures composed of different 2D materials can be found. Hexagonal boron nitride (h-BN) crystals are used as substrates or encapsulation layer for graphene because of their insulating property. However, it turned out that h-BN is not phys-

* Corresponding authors at: Department of Physics, Ulsan National Institute of Science and Technology (UNIST), Ulsan 44919, Republic of Korea (K. Kim), Department of Mechanical Engineering, Hanyang University, Ansan, Gyeonggi 15588, Republic of Korea (W.C. Lee), School of Chemical and Biological Engineering, Seoul National University, Seoul 08826, Republic of Korea (J. Park).

E-mail addresses: kpkim@unist.ac.kr (K. Kim), wonchullee@hanyang.ac.kr (W.C. Lee), jungwonpark@snu.ac.kr (J. Park).

http://dx.doi.org/10.1016/j.flatc.2017.07.004
2452-2627/© 2017 Elsevier B.V. All rights reserved.

Please cite this article in press as: J. Yang et al., Self-organized growth and self-assembly of nanostructures on 2D materials, FlatChem (2017), http://dx.doi.org/10.1016/j.flatc.2017.07.004

ically inert towards graphene. The lattice mismatch and orientation misalignment between h-BN and graphene induce periodic potentials that affect the density of states around their moiré patterns (Fig. 2) [8]. The superlattice of Dirac points, which are emerged at an energy depending on the moiré wavelength, result in the reduction of Fermi velocity with anisotropic transport characteristics. In addition, the graphene/h-BN heterostructures exhibit a commensurate-incommensurate transition depending on the relative lattice orientation [9]. A similar behavior is observed in the heterostructures constructed from 2D organic and inorganic nanostructures with metallic, insulating, or semiconducting properties. Consequently, manipulating the relative crystallographic orientations between the constituent materials becomes a prerequisite for rational designing of heterostructures with controlled physical properties.

Many kinds of nanostructures with different dimensionality (from 0D to 3D) have been assembled on 2D materials (reviewed in [10–13]), thus providing numerous ways of forming a range of heterostructures showing synergetic characteristics, which cannot be conventionally obtained from the parent materials. Among the different methods for fabricating heterostructures based on 2D materials, the direct chemical growth of nanostructures on a 2D substrate is the widely used method that offers opportunities to fabricate sophisticated heterostructures rationally, but with less effort, since the conventional synthetic procedure can be directly applied or modified in the presence of the host 2D material. More importantly, by controlling the reaction conditions for the growth of the nanostructures, the growth kinetics can be tuned to the extent where the van der Waals interaction between the nanostructure and the 2D material is exploited to spontaneously drive the growth to occur along specific crystallographic directions. As an origin of van der Waals interactions is from the atomic interactions between materials, hence, the self-organized growth of nanostructures follows the atomic arrangement of the host 2D material (Fig. 1). Such self-aligned heterostructures can enhance the coupling of the constituent materials in a desired manner.

In this review article, we summarize recent research on the self-organized growth and self-assembly of different nanostructures on 2D materials. A variety of self-organized structures such as organic molecules, inorganic nanomaterials, and 2D materials on different host 2D materials are respectively introduced in the following sections. We also highlight the assembly of various nanostructures on the 2D moiré periodic potentials of the 2D materials. Furthermore, we discuss the strategies for utilizing the self-organized growth behavior for application in advanced nanofabrication and mapping the crystal domains of 2D materials.

Self-assembly of organic molecules on 2D materials

In this section, we briefly discuss the self-assembly behaviors of organic molecules on various 2D materials (graphene, h-BN, and MoS_2). 2D materials possess atomically flat surfaces without dangling bonds, which facilitate well-organized molecular assembly. The assembly of organic molecules exhibits complex behaviors than does the assembly of atoms. The molecule itself has a non-isotropic shape and the molecular crystals can adopt various polymorphic structures depending on the molecular packing. On the surface, due to the subtle competition of molecule-molecule interaction vs. molecule-substrate interaction, the molecular assembly often adopts a nontrivial packing structure [14–17]. Moreover, the strength of the molecule-molecule interaction strongly depends on the type of molecule. For example, hydrogen-bonding between molecules can enhance the inter-molecular interactions [18]. These factors come into play during molecular assembly and result in various meta-stable configurations. Mechanically exfoliated flakes or chemically synthesized 2D materials, which are often transferred on insulating substrates (for example, SiO_2/Si), can be used for the epitaxial assembly of organic molecules. For some studies, suspended 2D membranes are prepared for organic molecular assembly, in which the underlying substrate effect on the assembly can be effectively removed.

Organic molecular assembly on graphite

For decades, graphite has been the most popular substrate for studying the assembly behaviors of various atoms and organic

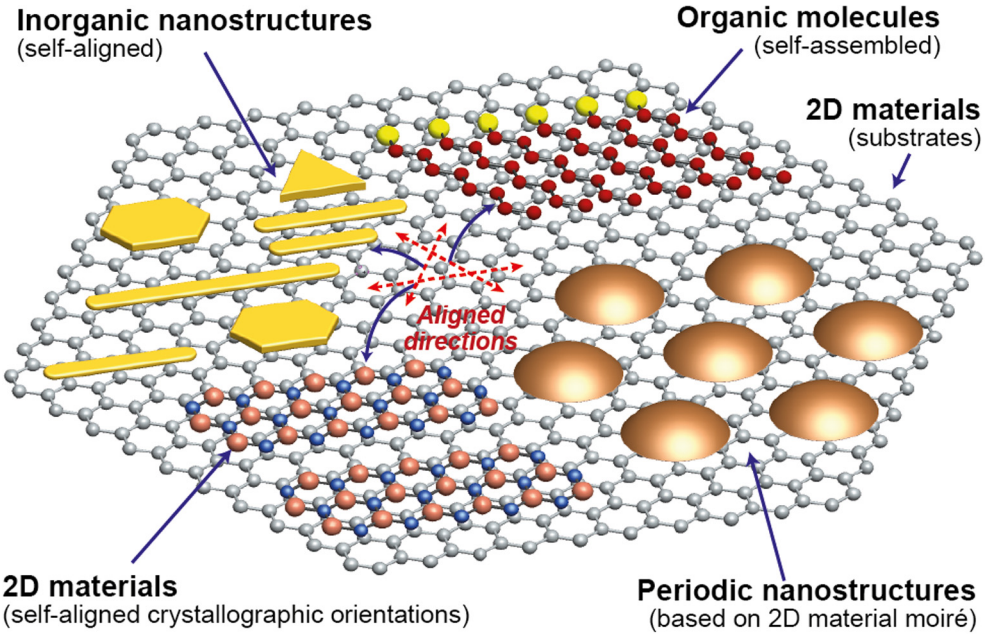

Fig. 1. Self-organized growth and self-assembly of nanostructures on 2D materials. This review categorizes a wide range of approaches in this research area into 4 groups, which are organic molecules self-assembled on 2D materials, inorganic nanostructures self-aligned on 2D materials, 2D materials self-aligned on 2D materials, and periodic nanostructures based on 2D material moiré.

Please cite this article in press as: J. Yang et al., Self-organized growth and self-assembly of nanostructures on 2D materials, FlatChem (2017), http://dx.doi.org/10.1016/j.flatc.2017.07.004

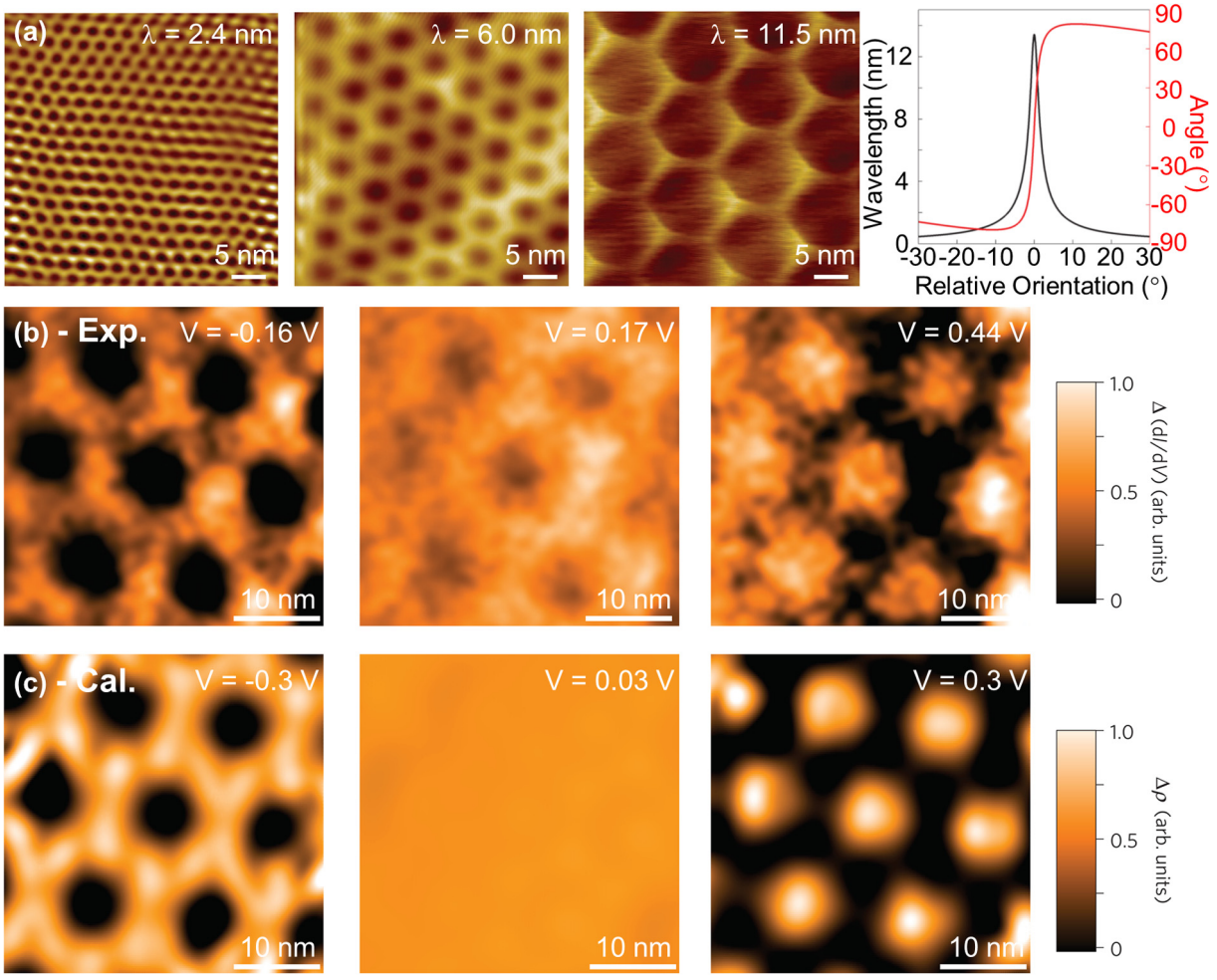

Fig. 2. (a) Scanning tunneling microscope topography images showing 2.4 nm, 6.0 nm and 11.5 nm moiré patterns of the graphene on h-BN. The right graph shows the superlattice wavelength (black) and rotation (red) depending on the angle between the graphene and h-BN crystals. (b) Experimental mapping images of the local density of the states for a 13.4 nm moiré patterns of the graphene/h-BN under −0.16 V, 0.17 V, and 0.44 V. (c) Theoretically calculated mapping images of the local density of the states for a 13.4 nm moiré patterns of the graphene/h-BN under −0.3 V, 0.03 V, and 0.3 V. [8], Copyright © 2012, Rights Managed by Nature Publishing Group.

molecules. Due to its flat and inert surface as well as its electrical conductivity, graphite has served as an ideal substrate for molecular resolution imaging by scanning tunneling microscopy (STM) [14,19–21]. This aspect is closely related to the emergence of recent research interest in molecular assembly on graphene. Generally, the assembly behavior of organic molecules on graphite can simulate the molecular assembly on graphene, although some reports indicate that molecular adsorption depends on the thickness of graphene. Various small organic molecules and polymers show well-aligned assemblies on graphite substrates. For example, pentacene, para-hexaphenyl (6P), and other such molecules formed well-ordered crystallites on graphite [22–24]. Zhang et al. has also reported the epitaxial growth of peptide nanofilaments on graphite, where the filament axes were aligned along the zigzag lattice direction of the underlying graphite [25].

Organic molecular assembly on epitaxial graphene (without strong moiré potential)

Researchers have been using various metallic and insulating single crystals for graphene (and h-BN) growth [26]. These so-called epitaxially grown graphene (or h-BN) substrates can be utilized for organic molecular assembly. Due to the lattice parameter mismatch between graphene and the growth substrate, the epitaxially grown graphene (and h-BN) forms a moiré pattern. Interestingly, the degree of surface corrugation related to the moiré patterns dramatically changes depending on the strength of the graphene-substrate interaction. For example, in the case of graphene grown on Ru, G/Ru(0001), the moiré periodic potential is very significant in that it strongly affects the molecular adsorption behavior. The formation of periodic nanostructures using the moiré potential will be discussed in the another section. Here, we discuss the assembly of organic molecules on epitaxial graphene without any (or a very weak) periodic potential.

When the interaction between graphene and the underlying substrate is weak, graphene moirés on substrates show a less pronounced surface corrugation. The flat surface of graphene facilitates the ordered assembly of organic molecules. For example, C_{60} molecules can form well-ordered crystallites on G/SiC(0 0 0 1) [27,28]. A well-defined directional alignment of C_{60} crystals relative to the graphene substrate direction was also observed on G/Cu(1 1 1) [29]. In this case, the C_{60} crystal facets are aligned along the graphene zigzag lattice direction, which forms a (4×4) superstructure arrangement. Even though there is some azimuthal preference for C_{60} crystal formation, the molecular structure shows a broad azimuthal distribution.

Many molecules exhibit a well-ordered assembly structure with long-range order, but without a precise azimuthal alignment on the graphene moiré. Perylene-3,4,9,10-tetracarboxylic dianhydride (PTCDA) molecules on G/SiC(0 0 0 1) showed well-ordered

Please cite this article in press as: J. Yang et al., Self-organized growth and self-assembly of nanostructures on 2D materials, FlatChem (2017), http://dx.doi.org/10.1016/j.flatc.2017.07.004

monolayer packing structures [30]. However, it appears that the azimuthal relation between PTCDA and epitaxial graphene is not well defined. Similarly, supramolecular porous networks using dehydrobenzo[12]annulene (DBA) were formed on G/SiC, but the azimuthal relation was not studied in detail [31]. Moreover, the adsorption of various phthalocyanine (Pc) on G/Ir(1 1 1) has been studied, which reveals a weaker template effect compared to that observed for G/Ru(0 0 0 1) [32].

Organic molecular assembly on transferred graphene

We will now briefly discuss the assembly of organic molecules on transferred graphene. Among the various small organic molecules, pentacene is one of the most intensively studied. Researchers have found that pentacene on chemical vapor deposited (CVD) graphene [33], when transferred on SiO_2, adopts a face-on molecular orientation due to the strong $\pi - \pi$ interaction between pentacene and graphene [34]. This study has also revealed the critical role of poly(methyl methacrylate) (PMMA) residue on graphene in determining the molecular assembly behavior [34]. TEM and selective-area electron diffraction (SAED) were performed to precisely determine the pentacene assembly structure on graphene (Fig. 3a–c) [35]. The facets of pentacene crystallites showed azimuthal alignment on graphene with 17° misorientation relative to the graphene zigzag lattice direction (Fig. 3a). SAED, together with the reconstructed molecular model, shows that the molecular axis of pentacene is aligned along the zigzag lattice direction. Moreover, the pentacene molecular axis is tiled by 17° in the molecular crystallites [35] (Fig. 3b and c). Similar crystallite alignments were also observed by SEM and optical microscope imaging for pentacene and other oligomeric crystallites [36,37]. The direction of alignment of perfluoropentacene on graphene/quartz was studied by grazing incidence X-ray diffraction (GIXD) [38], which revealed preferential molecular alignment along the zigzag and armchair directions of the underlying graphene substrate.

The alignment of C_{60} crystals on CVD graphene was also investigated by TEM and SAED (Fig. 3d–f) [39], which revealed preferential alignment of the C_{60} facets along the zigzag and armchair lattice directions of graphene. The somewhat broadened angular

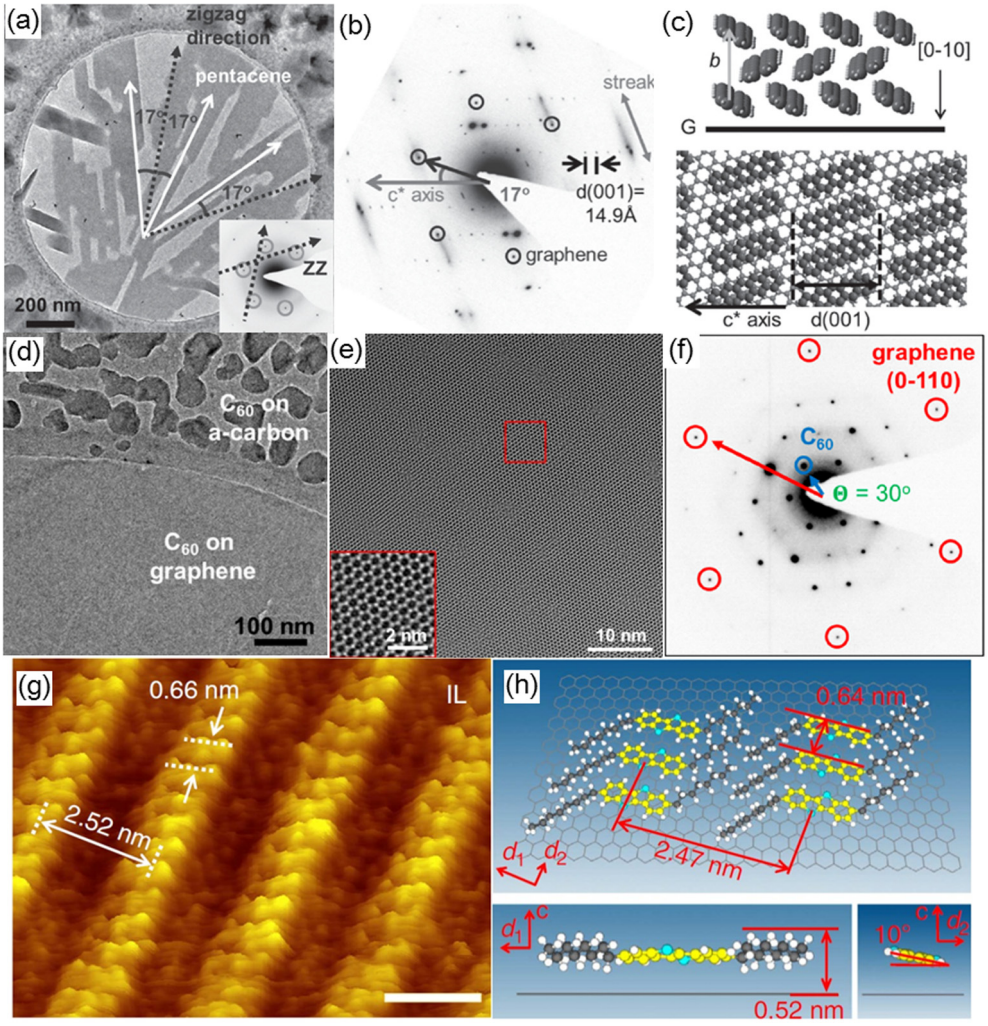

Fig. 3. Organic molecular assembly on transferred graphene. (a) TEM image of pentacene crystals on graphene. Inset shows the electron diffraction of underlying graphene membrane. The axes of pentacene crystals have a relative misorientation Θ of 17° from the graphene zigzag directions. (b) Selected area electron diffraction (SAED) of strained pentacene crystal on graphene. The diffraction signals marked by circles are graphene (0–110) spots. The c^*-axis is aligned with a pentacene crystal axis. (c) Molecular packing structure on graphene with zone axis [0–10]. Bottom image shows a top view of the pentacene film on graphene. (d) TEM image of C_{60} film on graphene membrane and around the edge of a hole in a Quantifoil TEM grid. (e) Zoomed-in TEM image of C_{60} film on graphene membrane. The uniform lattice structure of C_{60} is visible. Red square is a field of view for the inset. (f) SAED of C_{60} grown on graphene. (g) A constant-current STM image of the IL on CVD graphene. Scale bar: 2 nm. (h) Top view (top panel) and side view (bottom panels) of the most stable IL structure obtained by density function theory calculations. (a)–(c) [35], Copyright © 2015, WILEY-VCH Verlag GmbH & Co. KGaA, Weinheim. (d)–(f) [39], Copyright © 2015, American Chemical Society. (g) and (h) [41], Copyright © 2014, Rights Managed by Nature Publishing Group.

Please cite this article in press as: J. Yang et al., Self-organized growth and self-assembly of nanostructures on 2D materials, FlatChem (2017), http://dx.doi.org/10.1016/j.flatc.2017.07.004

distribution of the crystal directions was attributed to the non-ideal surface conditions, such as possible PMMA residues. Two-dimensional crystal of phosphonic acids on G/SiO_2/Si was also observed [40]. AFM imaging revealed the preferred directional growth of the molecular crystals, while theoretical calculations indicated that the molecular chain was aligned to the zigzag graphene lattice direction. In addition, the epitaxial growth of 2,7-dioctyl[1]benzothieno[3,2-b][1]benzothiophene (C_8-BTBT) single-crystal on exfoliated graphene was demonstrated (Fig. 3g and h) [41]. The first layer of C_8-BTBT has a lying-down molecular geometry, while the second layer has a standing geometry due to a weak molecule-substrate interaction. Other examples of the epitaxial alignment of organic crystals include n-hexatriacontane (HTC, $C_{36}H_{74}$) and lauroyl peroxide nanowires [42,43]. Graphene transferred onto h-BN shows a more uniform surface compared to that of G/SiO_2/Si, and can enhance the ordering of molecular assembly, as demonstrated by the case of cobalt phthalocyanine (CoPc) [44]. Although CoPc forms a well-ordered square lattice, it does not show orientation ordering as shown by the underlying graphene.

Polymeric materials as well as strongly bonded organic frameworks also show a well-ordered assembly structure on graphene. Electron diffraction data indicate that PMMA forms a two-dimensional packing structure on suspended graphene, in which the polymer backbone direction is aligned to the zigzag lattice directions of graphene [45]. Moreover, covalent organic frameworks (COFs) can exhibit excellent 2D growth behavior; however, the degree of azimuthal alignment of the COFs relative to that of the graphene substrate is not known [46].

Organic molecular assembly on transferred h-BN

Recently, h-BN has attracted much attention as a molecular assembly template. Particularly, h-BN being an electrical insulator, can serve as a dielectric substrate for electrical applications. Lee and co-workers have demonstrated the epitaxial growth of single-crystal rubrene on exfoliated h-BN flakes (Fig. 4a) [47]. Crystal structure information, as obtained by TEM and GIXD, reveals the azimuthal angle between the a-axes of rubrene and the h-BN zigzag lattice direction at 4°. Epitaxial alignment of needle-like crystallites of 6P was observed on h-BN flakes (Fig. 4b) [48]. The long axes of the needles were oriented 5° off from the h-BN zigzag direction. The epitaxial growth of pentacene thin films on h-BN was also investigated (Fig. 4c and d) [49]. AFM and TEM analysis confirmed the epitaxial growth behavior on h-BN, wherein 16° rotation of the molecular diffraction peak corresponding to h-BN diffraction was observed, similar to the case of pentacene on graphene. Moreover, using this system, researchers investigated the molecular-layer-thickness dependence of charge transport. In other study, the epitaxial alignment of C_{60} crystals on CVD-grown h-BN has been studied using TEM and SAED [50].

Organic molecular assembly transferred on other 2D crystals

Although organic molecular assembly on emerging 2D crystals such as MoS_2 and other transition metal chalcogenides has gained much attention very recently, the number of studies on this topic is still very limited. More than 20 years ago, STM imaging have

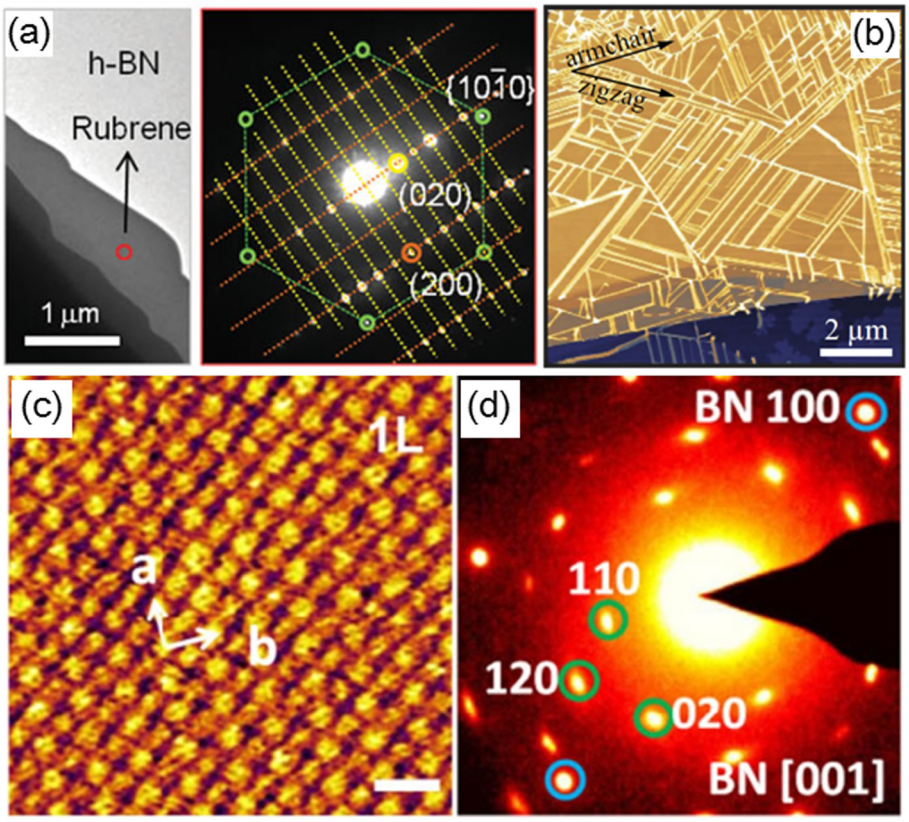

Fig. 4. Organic molecular assembly on transferred h-BN. (a) Bright-field TEM image and SAED pattern of the rubrene crystal grown on h-BN. The rubrene (2 0 0) and (0 2 0) and h-BN (10–10) planes are indicated by orange, yellow, and green circles, respectively. (b) AFM topography image of 6P crystallite on h-BN flakes. The arrow indicates high-symmetry directions of the supporting h-BN flakes. (c) High-resolution AFM image of a 1 L pentacene crystal on h-BN. Scale bar: 1 nm. (d) SAED pattern of a few-layer pentacene sample. Blue circles mark the h-BN (1 0 0) directions and green circles mark the pentacene (1 1 0), (1 2 0), and (0 2 0) directions. (a) [47], Copyright © 2014, WILEY-VCH Verlag GmbH & Co. KGaA, Weinheim. (b) [48], Copyright © 2016, Rights Managed by Nature Publishing Group. (c) and (d) [49], Copyright © 2016, American Physical Society.

Please cite this article in press as: J. Yang et al., Self-organized growth and self-assembly of nanostructures on 2D materials, FlatChem (2017), http://dx.doi.org/10.1016/j.flatc.2017.07.004

already demonstrated the ordered molecular assembly on MoS_2 [51,52]. Recently, the aligned growth of polydiacetylene (PDA) with 11° misorientation on MoS_2 has been observed (Fig. 5a and b) [53]. Moreover, phosphonic acid crystals were grown on MoS_2 substrate [54], where the directional growth of molecular crystals with 12° misorientation between different grains were observed from AFM analysis [54]. This misorientation was attributed to the presence of grain boundaries in the MoS_2 substrate; however, the experimental data on the precise epitaxial relationship relative to the MoS_2 substrate was not provided. PTCDA self-assembly on single-layer WSe_2/graphite has been investigated by STM [55]. The formation of a well-ordered herringbone packing structure by PTCDA has also been reported, in which there was no apparent orientation alignment between the PTCDA ad-layer and the WSe_2 substrate [55].

Inorganic nanostructures self-aligned on 2D materials

The previous section describes the formation of self-ordered structures by organic molecules on 2D materials owing to the direct interaction (non-covalent interaction) between the organic molecules and the pristine surfaces of the 2D substrates, wherein the atomically ordered structures of the 2D materials are projected on to the organic molecules. On the other hand, due to the chemical inertness of the 2D material surfaces, most of the inorganic materials preferentially attach to the edges and defects in the 2D substrates, thus forming randomly scattered particles on 2D materials [13]. However, several studies have reported self-organized structures of inorganic materials on 2D substrates, which are introduced in this section. They are also summarized in Table 1.

Van der Waals epitaxy of inorganic compounds on 2D materials

2D material surfaces do not possess dangling bonds. Koma et al. have been studying the epitaxial growth on such surfaces since the 1990s [56]. They attempted the fabrication of well-ordered or well-aligned patterns of inorganic materials on the cleaved face of a layered material such as mica. Because the heteroepitaxial growth proceeds due to the van der Waals interaction between the substrates and molecules, the process was named as van der Waals epitaxy or van der Waals heteroepitaxy.

After the concept of 2D material (especially graphene) was suggested, researchers started to replace the substrate of van der Waals epitaxy from the cleaved face of layered materials to 2D materials. Dang et al. suggested one of the first studies where bismuth selenide (Bi_2Se_3) was deposited on few-layered graphene [57]. The deposited bismuth selenide forms thin plates with triangular or hexagonal shapes whose edges are preferentially oriented along three directions with rotations of 120° relative to one another. (Fig. 6a and b) The three directions are the armchair lattice directions of the underlying graphene in real lattice space.

Indium arsenide (InAs) also shows similar self-alignment on graphene. (Fig. 6c and d) Hong et al. published a series of papers [58–60] on the self-aligned structures of InAs on graphene and cleaved graphite flakes. InAs forms vertical nanowires on graphitic surfaces (including single-layered graphene), with their edges (nanowire sidewall) preferentially oriented along the zigzag lattice directions of the underlying graphene in real lattice space. They also fabricated epitaxial InAs/graphene/InAs double heterostructures [58], where the single-layered free-standing graphene was sandwiched between two InAs layers. The epitaxial alignment between graphene and InAs was maintained in this structure. As a unique case, the remote epitaxial growth of GaAs on graphene/GaAs substrates has been recently demonstrated [61]. In this study, GaAs/graphene/GaAs heterostructures can be obtained by metalorganic chemical vapor deposition (MOCVD) of GaAs on graphene/GaAs substrates. Interestingly, the grown GaAs layer follows the crystal orientation of the underlying GaAs layer (i.e., homoepitaxial growth), because the ultrathin graphene cannot completely screen the potential field of GaAs substrates.

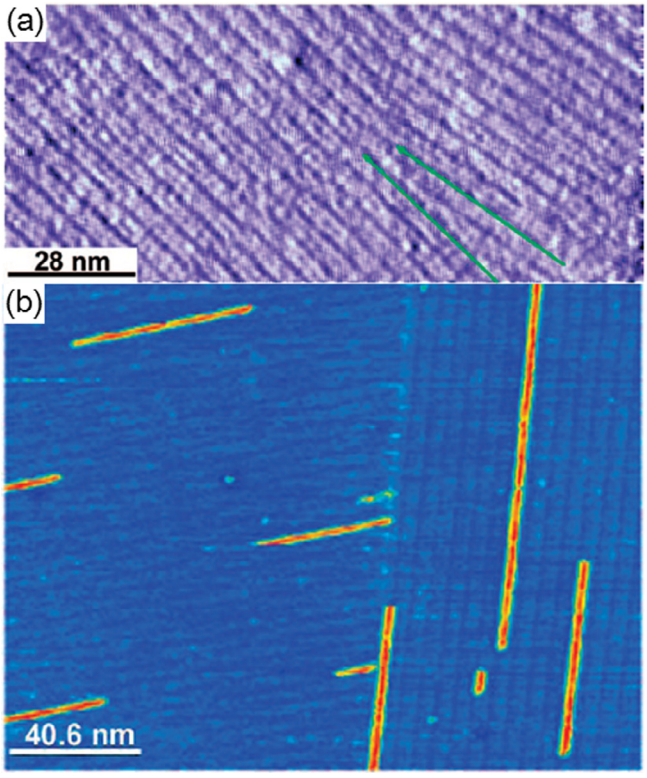

Fig. 5. Organic molecular assembly on MoS_2. (a) STM image of PCDA monolayers on MoS_2. (b) STM image of PDA wires on MoS_2. (a) and (b) [53], Copyright © 2008, American Chemical Society.

While the above studies are based on vapor-phase deposition at relatively high temperatures, liquid-phase synthesis can also form self-organized nanostructures on 2D materials. (Fig. 6e–h) In this regard, the most notable work is the aqueous-phase synthesis of AuCN (gold cyanide) nanowires on graphene [62,63]. Here, the nanowires synthesized at room temperature were highly aligned along the zigzag lattice directions of the underlying graphene, indicating that AuCN spontaneously binds and interacts with the pristine graphene surface. Recently, it was reported that uranium dioxide (UO_2) nanocrystals can be synthesized on graphene oxide using organic solvents [64]. The study showed the preferred orientations (3-fold symmetric orientations) of the UO_2 nanocrystal edges, although the alignment was poor, which might have originated from the imperfect structures of graphene oxide that was dispersed in an organic solvent for the nanocrystal synthesis reaction.

Self-aligned metal nanocrystals deposited on 2D materials

Certain kinds of metal nanocrystals seem to have self-aligned edges (aligned to the 3-fold symmetric directions) on 2D materials. (Fig. 7) The interaction between metals and graphene has traditionally been an important research topic [65,66], and a variety of metals have been deposited on graphene under various conditions [67–73]. Gold is known to form self-aligned nanocrystals on graphite [74], and it has been confirmed that similar alignment can be achieved on few-layered graphene [75,76]. These studies also indicate that geometries and densities of gold nanoparticles are strongly dependent on the number of graphene layers and

Please cite this article in press as: J. Yang et al., Self-organized growth and self-assembly of nanostructures on 2D materials, FlatChem (2017), http://dx.doi.org/10.1016/j.flatc.2017.07.004

Table 1
Representative examples of the self-aligned growth of inorganic nanocrystals (inorganic 3D nanocrystals and 2D materials) on 2D materials.

Nanocrystal characteristics			2D material (substrate)	Nanocrystal growth conditions		Alignment characteristics			Ref. #
Type	Material	Shape		Environment	Temperature	Lattice direction aligned to nanocrystal edges	Alignment error*	Lattice mismatch	
3D nanocrystal	Bi_2Se_3	Triangular or hexagonal plate	Graphene	Vapor	330 – 380 °C	Armchair	9.9° (Fig. 6a in this paper)	~2.9%	[57]
	InAs	Hexagonal column (vertical nanowire)	Graphene	Vapor	560 °C	Zigzag	12.2° (Fig. 6c in this paper)	~0.5%	[58–60]
	AuCN	Nanowire (lateral)	Graphene	Aqueous	~25 °C	Zigzag	3.7° (Fig. 2g in [63])	~3.3%	[62,63]
	UO_2	Hexagonal plate (thick plate)	Graphene (graphene oxide)	Organic solvent	200 – 330 °C	Zigzag	Large	~3.7%	[64]
	Au	Triangular or hexagonal plate	Graphene	Vapor	600 – 800 °C (Annealing)	Armchair	7.5° (Fig. 7a in this paper)	~1.4%	[74–76]
	Dy	Triangular or hexagonal plate	Graphene	Vapor	~390 °C	Not measured	10.2° (Fig. 7b in this paper)	Not discussed	[68,69]
	Eu	Hexagonal plate	Graphene	Vapor	~25 °C	Not measured	24.2° (Fig. 7c in this paper)	Not discussed	[68,69]
	Au	Nanowire (lateral)	MoS_2	Aqueous (Drying)	150 °C	Not measured	10.6° (Fig. 7e in this paper)	~8%	[77]
2D material	Graphene	Rounded hexagonal plate	h-BN	Vapor	500, 1000 °C	Zigzag	8.3°** (Fig. 1f in [85])	~1.8%	[83,85]
	MoS_2	Irregularly-shaped plate	h-BN	Vapor	400 – 800 °C	Cannot be obtained***		~24%	[86]
	WS_2	Not observed	h-BN	Vapor	400 °C	Cannot be obtained***		~26%	[103]
	MoS_2	Hexagonal plate	Graphene	Vapor	400, 900 °C	Zigzag	9.5° (Fig. 1a in [97])	~28%	[97]
	GaSe	Saw-edged plate	Graphene	Vapor	700 – 750 °C	Not clear (interlayer rotation: 10.9°)	8.4° (Fig. 1e in [90])	~50%	[90]
	WSe_2	Triangular or hexagram plate	Graphene	Vapor	950 °C	Armchair	8.2° (TOC Fig. in [97])	~23%	[97]
	$MoTe_2$	Dendritic plate	MoS_2	Vapor	25 – 350 °C	Cannot be obtained***		~5%	[106]
	MoS_2	Triangular plate	WS_2	Vapor	650, 850 °C	Cannot be obtained or defined (vertical or lateral heterostructures)		~1%	[99]
	WSe_2	Triangular or hexagonal plate	WS_2	Vapor	1190 °C	Cannot be defined (lateral heterostructures)		~4%	[100]

* The alignment error is defined as a standard deviation of nanocrystal edge orientations, which are obtained from the figures indicated in parentheses. Hexagonal symmetry is applied for the determination of crystallographic directions of underlying 2D materials.
** The actual value of alignment error may be larger than this value because the curved edges of graphene are assumed as straight lines in the measurement.
*** The original papers confirmed the crystallographic alignments between two 2D materials using SAED, LEED, or moiré patterns.

the growth (or annealing) temperature. The Tringides group published a series of papers [68–73] that showed STM images of various metal nanocrystals (Eu, Gd, Dy, Pb, and Fe) on graphene, which clearly demonstrate that the nanocrystal edges of Dy and Eu are aligned to the 3-fold symmetric directions of graphene [68,69]. The last example of self-aligned metals on 2D materials is different from the above examples. In this study, gold nanowires synthesized from aqueous solution were oriented along the six-fold symmetric directions of MoS_2 [77]. Their theoretical and experimental analyses revealed that the strong interaction between Au and S induced the oriented growth of gold nanowires.

Inorganic materials self-ordered by organic linker molecules

The above-mentioned cases are based on inorganic materials that interact directly with pristine surfaces of 2D materials. However, such inorganic materials are uncommon due to the chemical inertness of the 2D material surfaces. Another approach to aligning the inorganic materials on 2D materials is the use of organic molecules as linkers [78–81]. Because many organic molecules preferentially form self-assembled structures on 2D materials, as discussed in the previous section, inorganic materials that have affinity to specific parts of the organic molecules also form self-organized patterns on 2D materials. The idea was first presented by Zhang et al. using liquid-phase synthesis of Au nanoparticles on reduced graphene oxide (rGO) [78], where 1-octadecanethiol (ODT) was pre-adsorbed. In detail, the ODT molecules first formed a self-assembled herringbone structure on the rGO surfaces, following with the synthesized Au nanoparticles anchored to the thiol groups of the ODT molecules. Thus, the Au nanoparticles on the rGO surfaces formed dashed lines that were preferentially oriented along the three directions with rotations of 120° relative to one another. (Fig. 8a and b) Similar results were obtained using vapor-phase deposition of inorganic materials on PCDA (10,12-pentacosadiynoic acid) coated graphene [79]. The Hersam group published a series of papers [79,80] on the uniform deposition of high-*k* dielectric materials on graphene using organic linker molecules. They reported that ALD (atomic layer deposition) of zinc oxide (ZnO) or aluminum oxide (Al_2O_3) on PCDA-coated graphene generates line patterns along the armchair directions of the underlying graphene [79]. In conclusion, the method based on organic linker molecules can be expanded to the self-organization of various inorganic materials, although the indirect binding may reduce the orderliness of the self-organized patterns on 2D materials.

2D materials self-aligned on 2D materials

In this section, we summarize the recent progress in the self-organization of 2D materials on 2D materials. Although 2D materials are a part of inorganic nanomaterials discussed in the previous section, we dedicate this section for summarizing specific

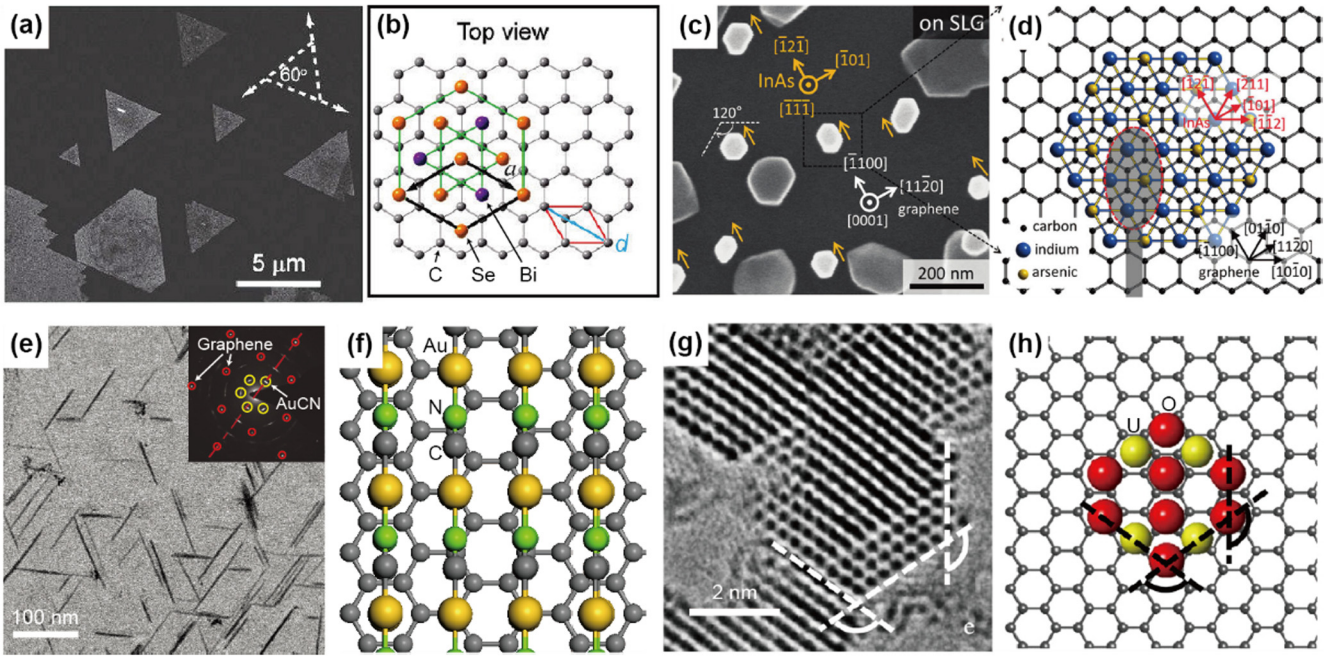

Fig. 6. Inorganic compounds self-aligned on graphene. SEM image (a) and atomic configuration (b) of Bi_2Se_3 nanoplates on few-layered graphene. SEM image (c) and atomic configuration (d) of vertical InAs nanowires on single-layered graphene. TEM image (e) and atomic configuration (f) of horizontal AuCN nanowires on single-layered graphene. TEM image (g) and atomic configuration (h) of UO_2 nanocrystals on graphene oxide. (a) and (b) [57], Copyright © 2010, American Chemical Society. (c) and (d) [60], Copyright © 2012, American Chemical Society. (e) and (f) [62] Copyright © 2015, Rights Managed by Nature Publishing Group. (g) and (h) [64], Copyright © 2016, Elsevier B.V.

examples of 2D materials self-organized on 2D materials because there recently have been huge efforts for the integration of 2D layered materials with other 2D layered materials to form 2D/2D heterostructures [1–3]. Since 2D layered materials have fully saturated chemical bonds on their surfaces, the neighboring 2D layered materials are assembled by the van der Waals forces, which is strong enough to hold them together because of their planar geometry with large surface areas. Because various 2D layered materials with unique characteristics are available, ranging from insulators to semiconductors and metals, a wide range of van der Waals 2D/2D heterostructures are possible. In this respect, chemical growth of 2D materials (bottom-up synthesis) on other 2D materials provides effective ways of creating high-quality 2D/2D van der Waals heterostructures. Another way of obtaining 2D/2D heterostructures is the mechanical transfer method, which can be categorized as a top-down approach. Because the scope of our review article is the self-organized growth on 2D materials, the mechanical transfer method is not discussed; however, readers

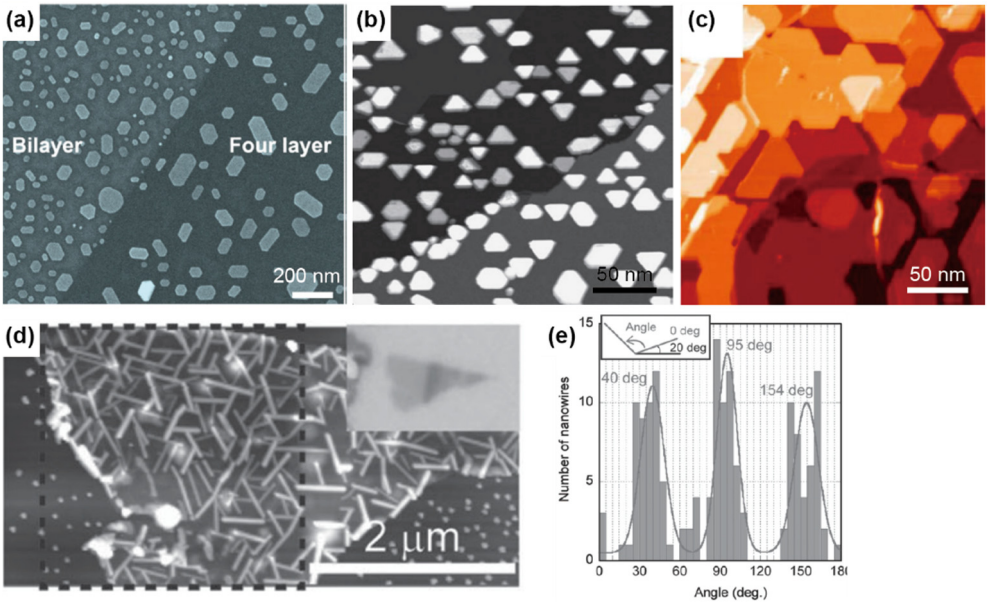

Fig. 7. Metals self-aligned on graphene and MoS_2. (a) SEM image of Au nanocrystals on few-layered graphene. (b) STM image of Dy nanocrystals on graphene/SiC(0001). (c) STM image of Eu nanocrystals on graphene/SiC(0001). (d) AFM image of horizontal Au nanowires on a single-layered MoS_2 surface. (e) Histogram of the Au nanowire orientations in (d). (a) [75], Copyright © 2013, Elsevier B.V. (b) [69], Copyright © 2011, WILEY-VCH Verlag GmbH & Co. KGaA, Weinheim. (c) [68], Copyright © 2010, American Physical Society. (d) and (e) [77], Copyright © 2015, WILEY-VCH Verlag GmbH & Co. KGaA, Weinheim.

Please cite this article in press as: J. Yang et al., Self-organized growth and self-assembly of nanostructures on 2D materials, FlatChem (2017), http://dx.doi.org/10.1016/j.flatc.2017.07.004

can find information on the mechanical transfer method from other review articles [1–3]. The representative examples of this section are summarized in Table 1.

Self-aligned CVD growth of 2D materials on h-BN

The most representative way of growing 2D nanostructures on another 2D layered material is the direct chemical vapor deposition (CVD) growth method. The direct CVD growth method has been successfully demonstrated (Fig. 9a) for the synthesis of 2D/2D van der Waals heterostructures such as graphene/h-BN [82–85], MoS_2/h-BN [86,87], MoS_2/graphene [88,89], and GaSe/-graphene [90]. Because the 2D materials are directly grown on other 2D layered materials used as substrates, the damage caused by mechanical transfer is avoided and the interfaces between the two 2D materials are clean. In addition, the bottom-up approach is intrinsically a scalable process, which is beneficial for the future commercial applications of these novel 2D/2D heterostructures. In spite of several advantages, the direct chemical growth method is limited by the number of possible combination of materials because of the sensitive growth conditions required by the 2D layered materials; this narrows the choice of substrates under the delicately controlled reaction parameters.

Graphene/h-BN heterostructures are one of the initially studied 2D/2D heterostructures, because the h-BN layers minimized the substrate effects that harmed the electronic properties of graphene [91]. It is known that substrate materials greatly affect the properties of graphene. For example, the carrier mobility of graphene decreases on SiO_2 substrates because of scattering caused by surface roughness, charged surface states, impurities, and surface optical phonons [92]. In addition, substrate disorders can induce the formation of inhomogeneous charge carrier puddles [93], which prevent the generation of 2D electron gas. Thus, the direct CVD growth method has been employed to form graphene/h-BN heterostructures by growing graphene on h-BN [83–85] or vice versa [82] (Fig. 9a and b). As demonstrated in the mechanically transferred graphene/h-BN heterostructures [91], chemically grown graphene on h-BN exhibits superior carrier motilities as high as 37,000 $cm^2 \cdot V^{-1} \cdot s^{-1}$ [84], which is comparable to that of the high-quality exfoliated graphene. Interestingly, there is a strong preference in the relative orientation between the grown 2D structures and the 2D materials that are used as substrates. In particular, when a graphene layer was grown on the h-BN crystals (or vice versa), it was found that both monolayer and bilayer graphene exhibited the same orientation with respect to the h-BN crystals (Fig. 9b) [83,85]. As discussed in the introduction, the relative alignment between two 2D materials is particularly important because it significantly affects the properties of the final heterostructures. The fixed relative crystal orientation (i.e., the self-aligned growth behavior) can be attributed to the epitaxial growth behaviors of the growing graphene layers (specifically, the van der Waals epitaxy mode [94]), and the small lattice mismatch between graphene and h-BN (<2%) might be helpful for the epitaxial growth.

It has been found that the small lattice mismatch is not always necessary for the self-alignment of 2D materials on other 2D materials. Among the various 2D materials, MoS_2 is an emerging 2D transition metal dichalcogenide material that has its own band gap. MoS_2 crystals can be successfully grown on h-BN crystals via CVD, although the lattice mismatch between MoS_2 and h-BN is as

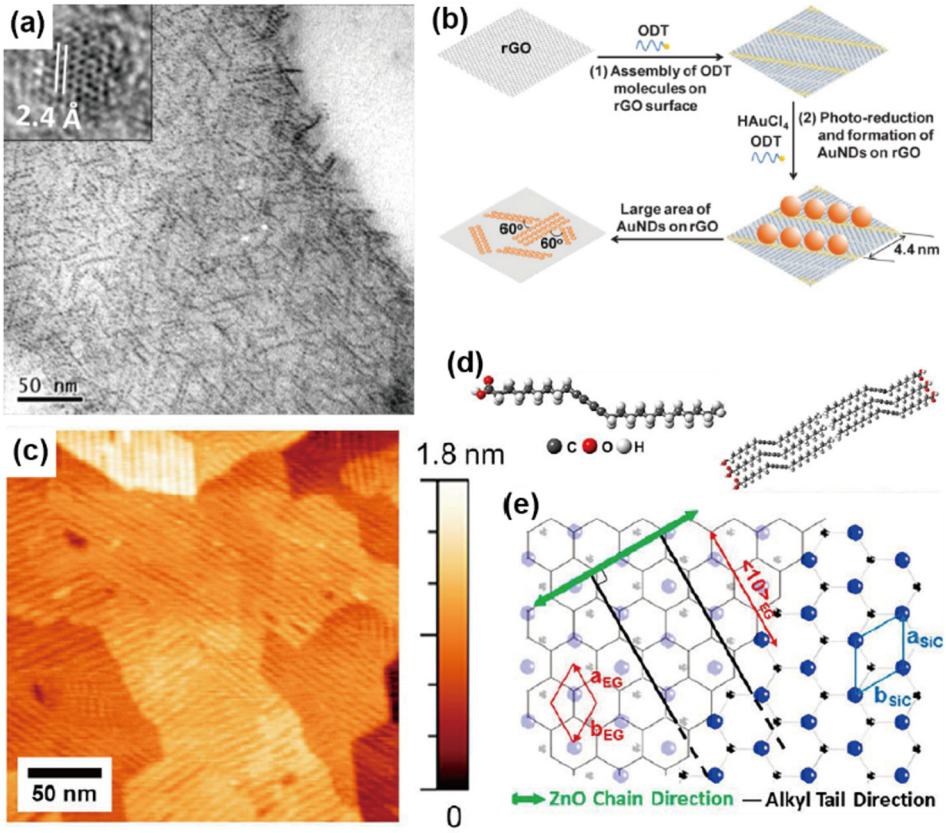

Fig. 8. Self-organized inorganic materials on graphene using organic linker molecules. (a) TEM image of 1-octadecanethiol capped Au nanoparticles synthesized on reduced graphene oxide. (b) Schematic illustration of the synthesis process for the Au nanoparticles in (a). (c) AFM image of ZnO deposited on a self-assembled layer of 10,12-pentacosadiynoic acid (PCDA) on epitaxial graphene. (d) Molecular and assembly structures of PCDA. (e) A diagram presenting directional relations among ZnO chains, alkyl tails, and graphene crystal structures. (a) and (b) [78], Copyright © 2010, WILEY-VCH Verlag GmbH & Co. KGaA, Weinheim. (c)–(e) [79], Copyright © 2013, American Chemical Society.

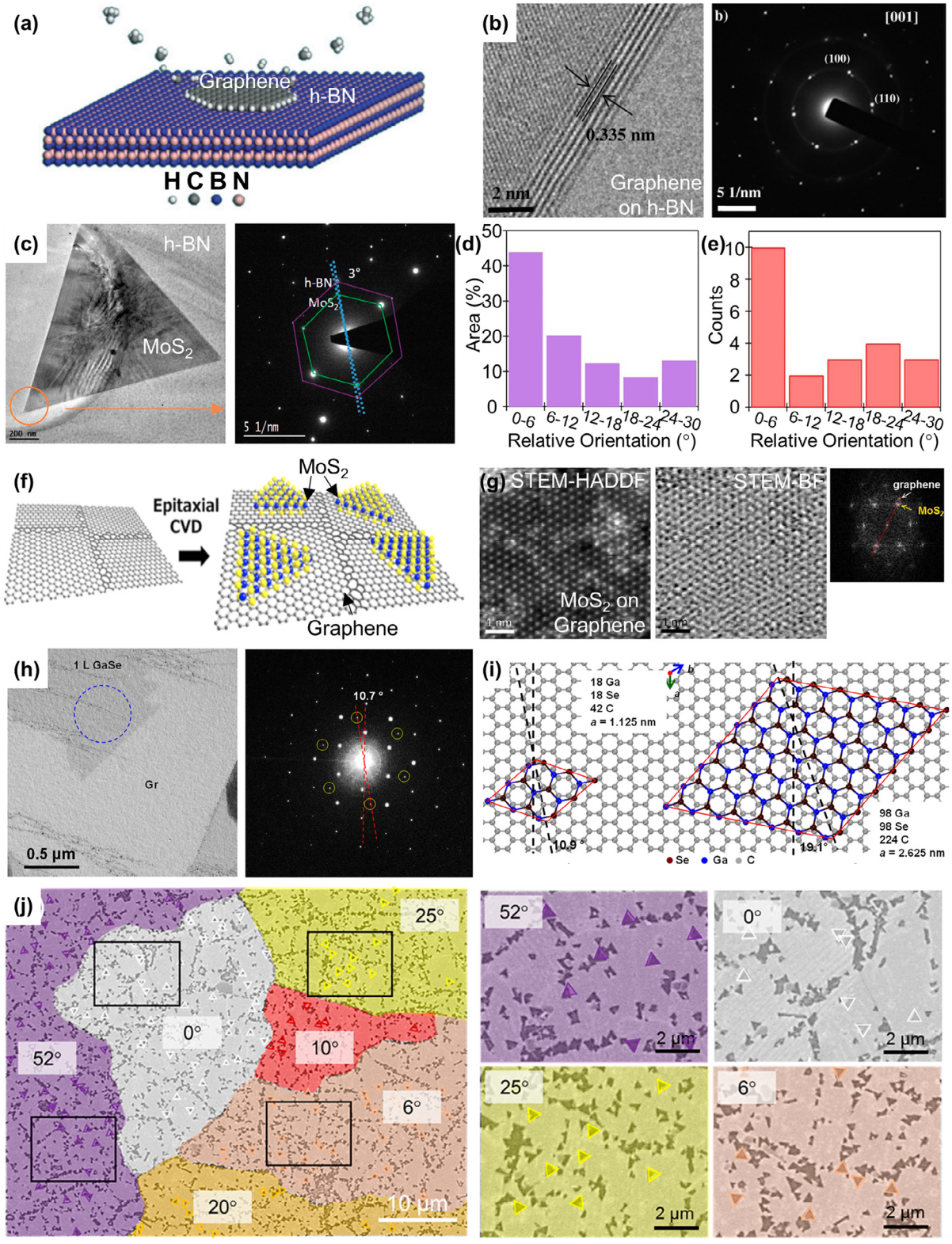

Fig. 9. Self-aligned growth of 2D nanostructures on 2D materials. (a) A schematic describing the CVD growth of graphene on h-BN. (b) High resolution TEM image of six layers of graphene on h-BN, and the selected area diffraction patterns of graphene/h-BN heterostructures. (c) TEM image and the corresponding diffraction patterns of the multilayer MoS_2 crystal grown on h-BN. The green and violet hexagons indicate the diffraction patterns of MoS_2 and h-BN, respectively. (d) Histogram showing the areal probability of monolayer MoS_2 crystals grown on h-BN with respect to the relative crystal orientation. (e) The count histogram of panel (d). (f) A schematic describing the CVD growth of MoS_2 on graphene. (g) Scanning TEM images of MoS_2 on graphene and the corresponding FFT patterns for the monolayer MoS_2 film grown on graphene. The red dashed line compares the crystal orientation. (h) TEM image and corresponding FFT pattern for GaSe grown on graphene. (i) Schematic showing the relative orientation of GaSe and graphene. (j) Visualization for the grain structure of polycrystalline graphene, which is determined by the orientation of MoS_2 grains. The figures on right show the high-magnification images of the areas enclosed in black squares. (a) [85], Copyright © 2013, Rights Managed by Nature Publishing Group. (b) [83], Copyright © 2011, Elsevier B.V. (c)–(e) [86], Copyright © 2015, American Chemical Society. (f) and (j) [97], Copyright © 2016, American Chemical Society. (g) [88], Copyright © 2012, American Chemical Society. (h) and (i) [90], Copyright © 2015, American Chemical Society.

Please cite this article in press as: J. Yang et al., Self-organized growth and self-assembly of nanostructures on 2D materials, FlatChem (2017), http://dx.doi.org/10.1016/j.flatc.2017.07.004

high as ~24% (Fig. 9c–e) [86,87], yielding MoS_2/h-BN heterostructures. For the self-organization of MoS_2 on h-BN substrates, two distinct formation mechanisms of MoS_2 crystals are proposed [86]: the screw dislocation-driven growth mechanism and the "layer-by-layer" growth mechanism [95,96] for mono and multilayer MoS_2, respectively. In addition, the self-aligned growth behavior is dominant for the MoS_2/h-BN heterostructures. As shown in the histograms (Fig. 9d and e), there is a preponderance of MoS_2 flakes with relatively low rotation angles (<6°), while there are only a few MoS_2 flakes that exhibit relatively high rotation angles of 12–30°. Moreover, the MoS_2 crystals on h-BN preserves their own band gap of ~1.89 eV, which is similar to that of the monolayer counterparts.

Self-aligned CVD growth of 2D materials on graphene

2D nanomaterials also successfully self-organize when graphene is used as the 2D substrate. Despite the huge lattice mismatch between MoS_2 and graphene (~28%), MoS_2/graphene heterostructures have been successfully obtained by the CVD growth method [88,89]. A schematic for the self-organization process of MoS_2 crystals on graphene is shown in Fig. 9f [97]. In a

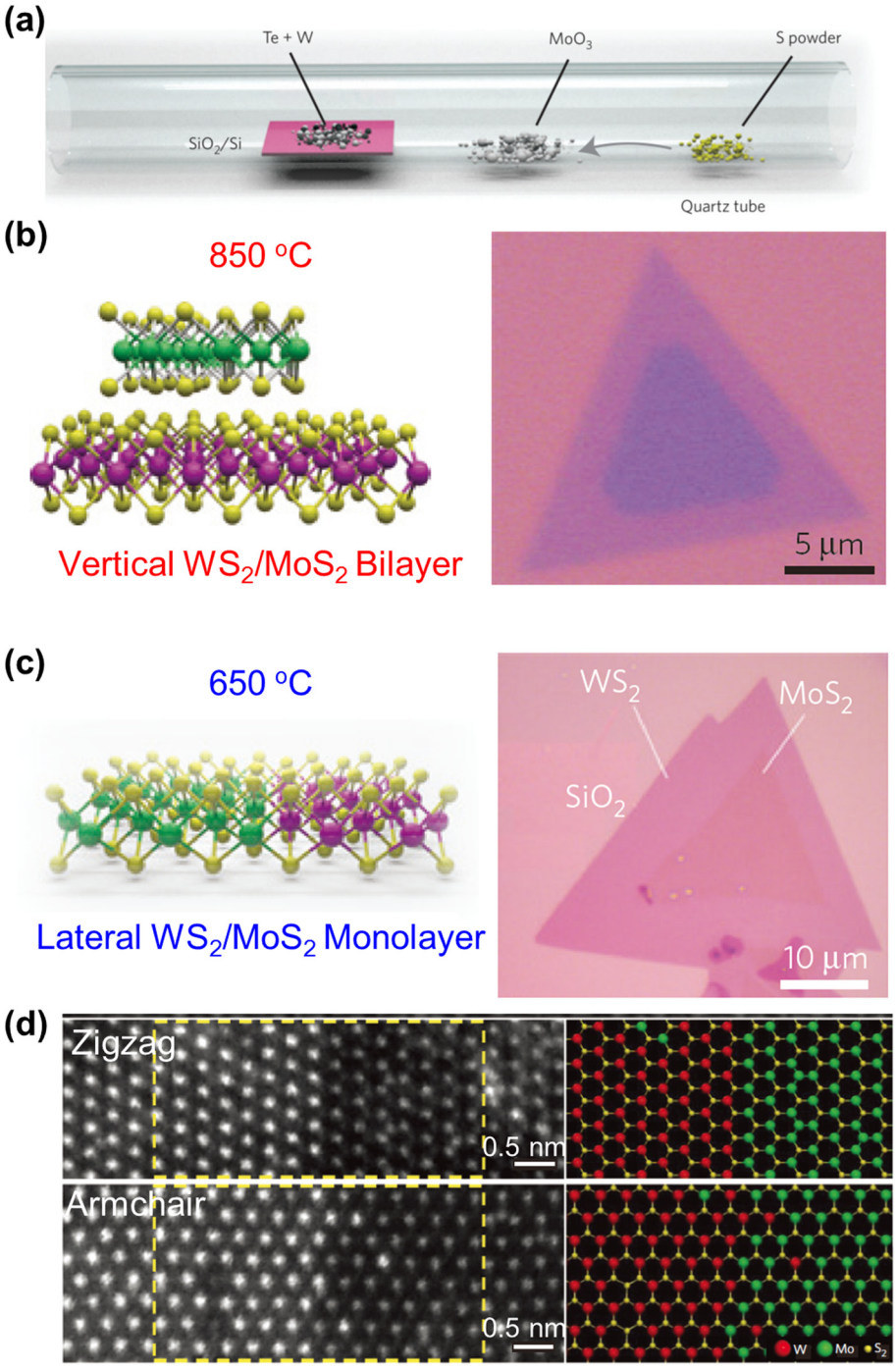

Fig. 10. Vertical and lateral growth of 2D/2D heterostructures. (a) A schematic of the synthesis of WS_2/MoS_2 heterostructures. (b) Schematic and optical images of the vertical growth of WS_2 crystals on MoS_2 crystals at 850 °C. (c) Schematic and optical images of the lateral growth of WS_2 crystals on MoS_2 crystals at 650 °C. (d) Atomic resolution Z-contrast scanning TEM images showing the WS_2/MoS_2 lateral interfaces along the zigzag and armchair directions. The atomic model is corresponding to the yellow-boxed region. The figure is reprinted with permission from [99]. Copyright © 2014, Rights Managed by Nature Publishing Group.

Please cite this article in press as: J. Yang et al., Self-organized growth and self-assembly of nanostructures on 2D materials, FlatChem (2017), http://dx.doi.org/10.1016/j.flatc.2017.07.004

study on the direct growth of MoS_2 on graphene [98], it was suggested that the formation of MoS_2 crystals starts at the curved sp^2 π bonds or the dangling bonds at the graphene boundaries, which act as nucleation sites. In spite of the huge difference in the lattice constants, MoS_2 layers grow in a specific direction with respect to the graphene substrate. The relative lattice orientation of the constituent layers was investigated by TEM. As seen in their FFT patterns (Fig. 9g), most of the MoS_2 grains are aligned within the narrow range of the orientation angle from −11 to 18° with respect to the graphene layers underneath [88]. Similarly, GaSe/-graphene heterostructures can be obtained by the self-organized growth of GaSe crystals on a graphene substrate (Fig. 9h). GaSe and graphene also exhibit a huge lattice mismatch of ~50%. Interestingly, the average relative rotation angle between GaSe and graphene is ~10.5° (Fig. 9i), which is in contrast to the general 2D/2D heterostructures where the two layered materials are aligned in the same direction. Theoretical analysis reveals that the rotation angle of 10.9° energetically stabilizes the GaSe/graphene heterostructures, as it results in small supercells with lowest strain and highest binding energy.

Based on the self-alignment relationship between MoS_2 and graphene, it is possible to observe the grain structure of the underlying 2D layered materials by epitaxially growing MoS_2 crystals (Fig. 9j) [97]. In this study, triangular MoS_2 crystals were grown on polycrystalline graphene (i.e., MoS_2/graphene) that had grains with various orientations and sizes. Because the triangular MoS_2 crystals were grown on graphene with a fixed relative orientation, they directly showed the orientation and size of the graphene grains (Fig. 9j). In addition, the grain boundaries of the graphene layers could be easily observed by the formation of MoS_2 crystals since they have a higher probability of growing at the grain boundaries. Since the grain boundaries of graphene acted as nucleation sites, the MoS_2 crystals were densely formed at the grain boundaries.

Other cases: lateral heterostructures, multiple heterostructures, and molecular beam epitaxy growth

The direct CVD growth method has been successfully employed to obtain a variety of heterostructures based on 2D materials. One of the most representative examples is the formation of the lateral

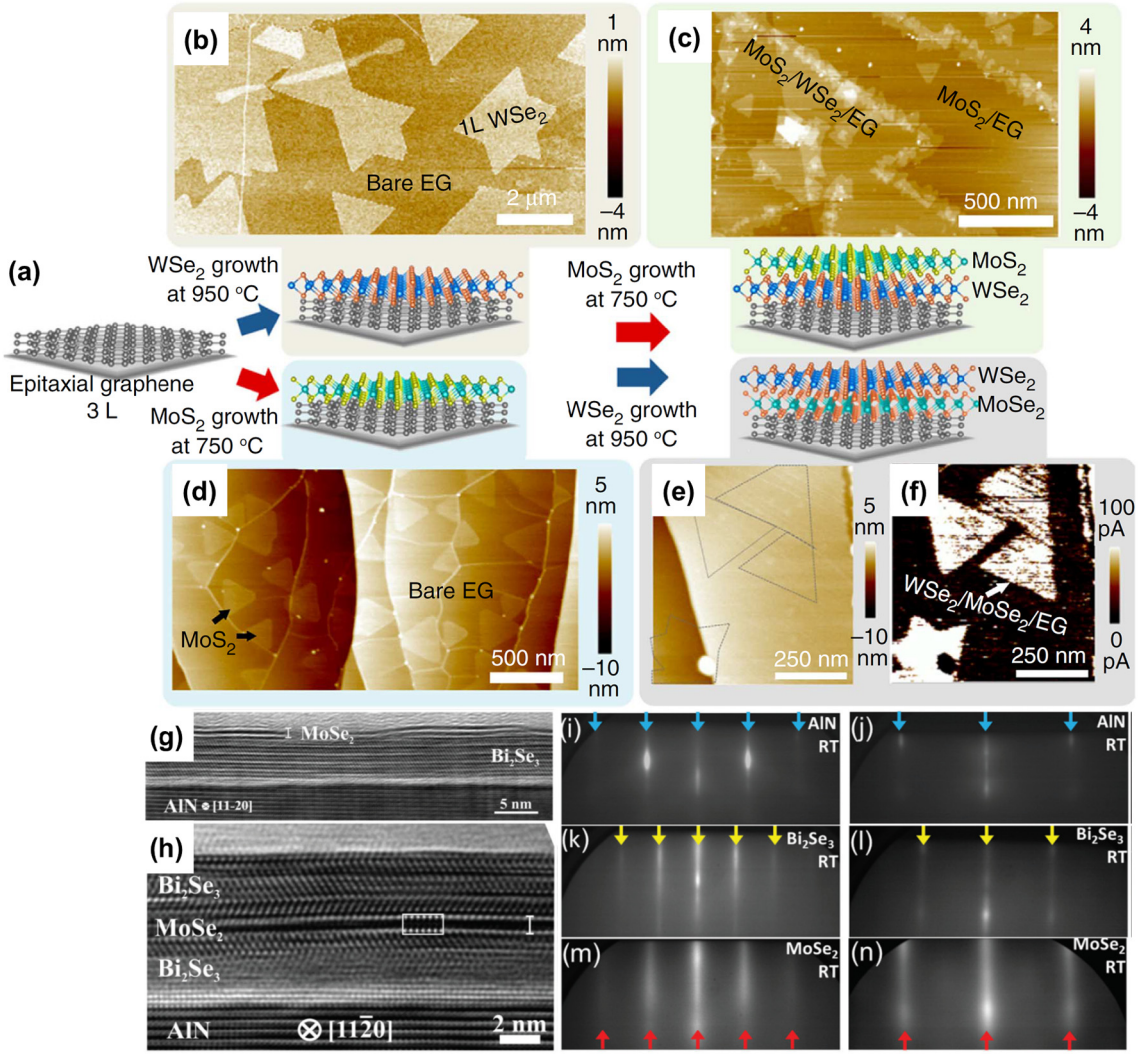

Fig. 11. Complex 2D/2D heterostructures. (a) A schematic showing the synthesis of MoS_2/WSe_2/graphene and WSe_2/MoS_2/graphene heterostructures. (b-e) Atomic force microscope images showing sequential growth of each layer: (b) MoS_2/WSe_2/graphene, (c) MoS_2/WSe_2/graphene, (d) WSe_2/MoS_2/graphene, and (e) WSe_2/MoS_2/graphene. (f) A conductive atomic force microscope image of panel e. (g,h) High-resolution TEM images of (g) 2 layer $MoSe_2$/5 layer Bi_2Se_3 and (h) 3 layer Bi_2Se_3/2 layer $MoSe_2$/3 layer Bi_2Se_3 heterostructures. (i-n) Reflection high-energy electron diffraction patterns of 2 layer $MoSe_2$/5 layer Bi_2Se_3 heterostructures on an AlN substrate. The blue, yellow, and red arrows show the AlN (substrate) and the Bi_2Se_3 and $MoSe_2$ streaks, respectively. (a)–(f) are reprinted with permission from [101], Copyright © 2015, Rights Managed by Nature Publishing Group. (g)–(n) are reprinted with permission from [107], Copyright © 2015, Royal Society of Chemistry.

Please cite this article in press as: J. Yang et al., Self-organized growth and self-assembly of nanostructures on 2D materials, FlatChem (2017), http://dx.doi.org/10.1016/j.flatc.2017.07.004

2D/2D heterostructures. By simply changing the reaction parameters, both vertical and lateral heterostructures of WS_2/MoS_2 monolayers can be synthesized from the 2D MoS_2 crystals (Fig. 10) [99]. At a high temperature (850 °C), WS_2 monolayers vertically grew on top of the MoS_2 layers, while at a low temperature (650 °C), WS_2 monolayers grew laterally at the edges of MoS_2 (Fig. 10a–c). Similarly, lateral heterostructures based on $MoS_2/MoSe_2$ and WS_2/WSe_2 that act as lateral *p-n* junctions have been also reported [100]. In contrast to the vertical heterostructures where two 2D materials are held by van der Waals forces, covalent bonds are formed between two 2D materials when the second 2D material is grown in the lateral direction. This might be the main reason why the formation of lateral heterostructures is limited for layered materials with low lattice mismatch (e.g., ~1% for WS_2/MoS_2 and ~4% for WS_2/WSe_2). In addition, the constituent 2D materials of the lateral heterostructures are aligned in the same direction (Fig. 10), thus minimizing defects or dislocations. In the lateral heterostructures of WS_2/MoS_2, TEM analysis showed that the WS_2 and MoS_2 grains shared the same crystal orientation with sharp interfaces along the zigzag and armchair directions (Fig. 10d) [99]. The sharp interface with the same crystal orientation minimizes their interfacial energy, which ultimately stabilizes the heterostructures.

Based on the same principle, a third 2D layered material can be successfully grown on the self-organized 2D/2D heterostructures by the CVD method, resulting in the formation of 2D/2D/2D multiple heterostructures. As an example, MoS_2 and WSe_2 crystals were grown on the self-organized WSe_2/graphene and MoS_2/graphene heterostructures, yielding MoS_2/WSe_2/graphene and WSe_2/MoS_2/-graphene, respectively (Fig. 11a–f) [101,102]. The self-aligned growth behavior can be easily observed in these multiple heterostructures. The second and third 2D materials showed almost similar crystal orientations with a relative rotation angle of less than 2°.

Because of the sensitive CVD growth conditions for 2D materials, the self-organization of a 2D material on another 2D material is limited in terms of the number of combinations of the constituent materials. Consequently, one of the important research objectives is the development of novel synthetic approaches for the direct synthesis of versatile 2D/2D heterostructures that are otherwise not easily obtained by CVD. For example, WS_2 crystals can be successfully grown on h-BN under ultra-high vacuum condition [103]. On the same line, it was demonstrated that sulfurization reaction of the metal layers can be utilized to fabricate vertical heterostructures of MoS_2/WSe_2 with vertically aligned layers [104]. Furthermore, molecular beam epitaxy (MBE) method has been employed for the chemical synthesis of 2D/2D heterostructures (e.g., graphene/h-BN [105], $MoS_2/MoTe_2$ [106], and $MoSe_2/Bi_2Se_3$ [107]). Regardless of the preparation method, self-alignment of the constituent 2D materials is observed (Fig. 11g–n), evidencing that this behavior is a result of the thermodynamic stabilization of the 2D/2D heterostructures, rather than that of a specific preparation method.

Summary of representative examples in the sections 2 and 3

Table 1 summarizes representative examples of inorganic nanomaterials and 2D materials self-organized on 2D materials. As shown in the two sections, edges of top nanomaterials (inorganic 3D and 2D nanocrystals) are self-aligned along directions of six-fold symmetry while their sizes and positions are randomly distributed. It is because molecular structures of 2D materials control the crystallographic orientations of the synthesized inorganic nanocrystals. To evaluate degrees of the directional alignment, we define an alignment error as a standard deviation of nanocrystal edge orientations, which are measured from the images of nanocrystal presented in the reference papers (hexagonal symmetry is applied for the determination of crystallographic directions of underlying 2D materials). We also summarize characteristics of nanocrystals, 2D materials, and synthesis conditions of each work. It is difficult to directly compare examples shown in this table since they have inherent differences in growth condi-

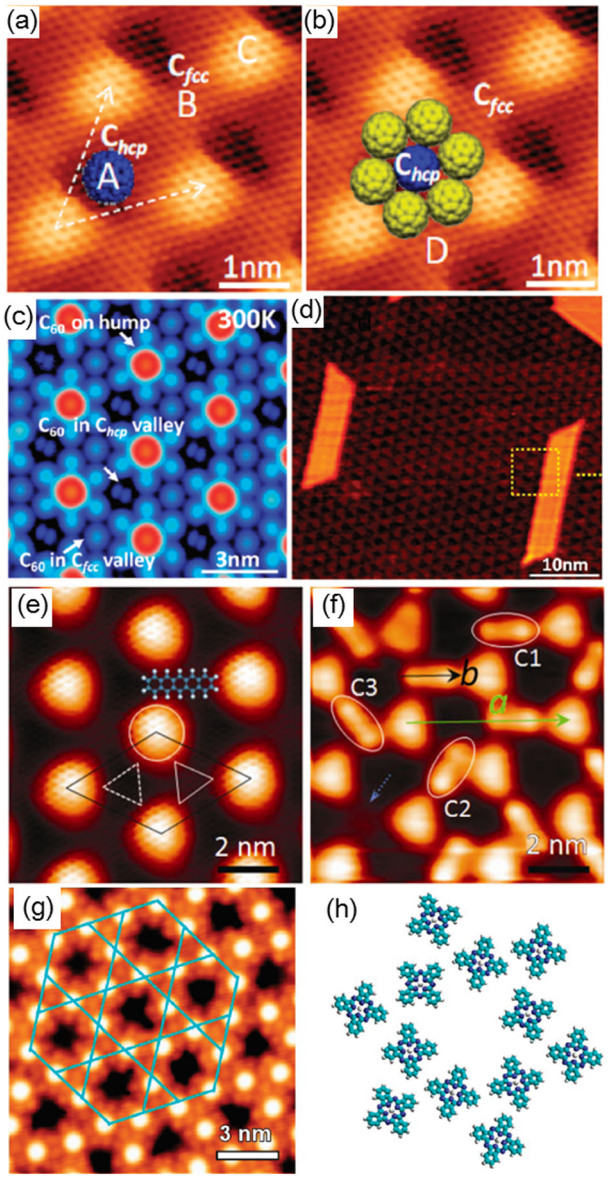

Fig. 12. Organic molecular assembly on G/Ru(0001) moiré pattern. (a) Scheme of an individual C_{60} molecule preferentially trapped in the C_{hcp} valley. (b) Scheme of six C_{60} molecules attached to the trapped C_{60} as a seed for the nucleation of monolayer C_{60} islands. (c) Molecularly oriented dumbbell-shaped features in the STM image of C_{60} molecules sitting in the C_{hcp} valley. (d) Homoepitaxial GNR with well-defined edges coexists and surrounds the polymerized C_{60} film. (e) STM atomic-resolution image of G/Ru(0001) with a rhombus indicating the moiré unit cell and a model of pentacene. Three distinct areas in the unit cell are outlined by solid circle (atop), solid triangle (fcc), and dashed triangle (hcp), respectively. (f) STM image showing pentacene molecules preferentially adsorbed on fcc regions. The ellipses indicate the three configurations. Vectors *a* and *b* are used to indicate the atop-atop direction of G/Ru and the long symmetric axis of pentacene, respectively. (g) STM image of the Kagome lattice of FePc. A trihexagonal tiling is highlighted. The unit cell of the Kagome lattice is indicated with blue lines. (h) Structural model of the Kagome lattice showing molecular orientation disorder. (a)–(d) [108], Copyright © 2012, American Chemical Society. (e) and (f) [111], Copyright © 2013, Tsinghua University Press and Springer-Verlag Berlin Heidelberg. (g) and (h) [112], Copyright © 2009, American Chemical Society.

tions and measurement processes. Nonetheless, this table should be helpful for readers to get general ideas about the self-organized growth of inorganic nanocrystals on 2D materials.

Nanostructure assembly on 2D moiré periodic potential

In this section, we briefly review the assembly of various nanostructures on the 2D moiré periodic potentials. 2D materials on atomically-ordered substrates often generate spatially periodic patterns (moiré patterns) of electronic potentials when the two materials have a small mismatch in lattice parameters. Because the electronic potentials modulate the deposition process of nanomaterials, periodic nanostructures can be formed on the 2D materials. As previously discussed in the section 1.2, the epitaxially grown graphene, such as G/Ru(0001), can exhibit a strong moiré corrugation, which results from the strong interaction between graphene and the underlying substrate. It is the moiré periodic potential, rather than the surface chemistry and the lattice structure of graphene and other 2D materials, that mainly drives the assembly of nanostructures, thus producing various interesting structures with spatial periodicity.

Organic molecular assembly using the strong moiré corrugation of G/Ru(0001)

The adsorption behaviors of organic small molecules and polymeric materials on graphene moiré have gained intensive interest recently. In the case of G/Ru(0001), researchers have observed a very strong template effect. For example, the hexagonal-close-packed (hcp) position in the G/Ru(0001) moiré is the favorite adsorption site for C_{60} (Fig. 12a and c) [108,109]. With increased coverage, the C_{60} molecules occupy different positions in the moiré pattern such as the face-centered-cubic (fcc) locations (Fig. 12b) [108]. With full coverage, the C_{60} molecules form a commensurate molecular structure on G/Ru(0001) as a result of lattice match between the C_{60} lattice and the G/Ru(0001) moiré pattern [108,109]. Researchers have also demonstrated that the polymerization of C_{60} assembly can lead to the formation of a well-defined carbon structure (Fig. 12d) [108].

Other organic molecules can also selectively adsorb on the graphene/Ru(0001) moiré. Selective adsorption of pentacene, Iron phthalocyanine (FePc), and other molecules has been observed on G/Ru(0001) (Fig. 12e–h) [110–113]. Moreover, various

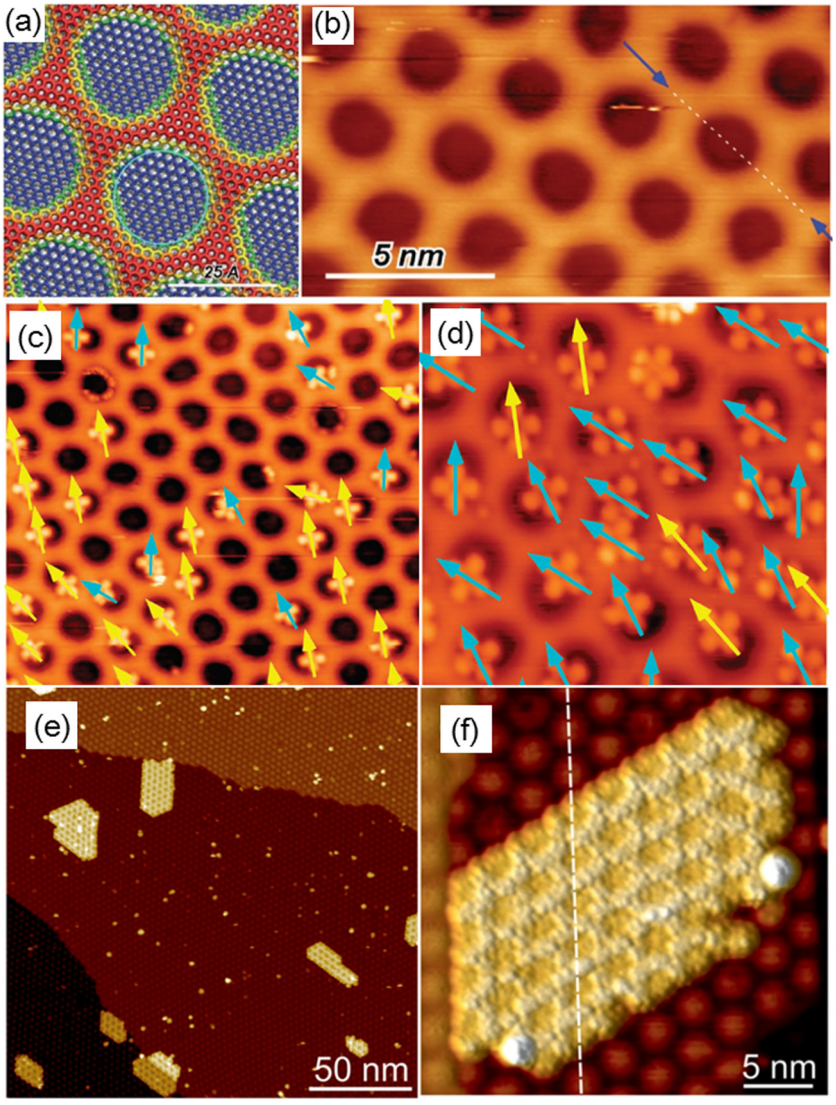

Fig. 13. Organic molecular assembly on h-BN/Rh(1 1 1) nanomesh. (a) Height color map of B and N atoms. (b) STM image of h-BN/Rh(1 1 1) nanomesh. (c) Constant current STM image of CuPc at 5 K adsorbed on a h-BN nanomesh. The arrows indicate the orientation direction of the molecules. (d) Constant current STM image of H_2Pc at 5 K adsorbed on a h-BN nanomesh. (e,f) STM topographic images of Fe_4H (0.06 ML) on h-BN/Rh(1 1 1). (a)–(d) [116], Copyright © 2014, Royal Society of Chemistry. (e) and (f) [117], Copyright © 2015, American Chemical Society.

Please cite this article in press as: J. Yang et al., Self-organized growth and self-assembly of nanostructures on 2D materials, FlatChem (2017), http://dx.doi.org/10.1016/j.flatc.2017.07.004

interesting assembly structures can be formed through selective adsorption on moiré positions. For example, with proper molecular coverage, FePc and other small organic molecules on G/Ru(0001) can form a Kagome lattice (Fig. 12g and h) [112].

Organic molecular assembly on epitaxially grown h-BN

Selective adsorption of organic molecules was also observed on epitaxially grown h-BN. h-BN grown on various metallic substrates also produces moiré patterns on the surface, which results from the lattice mismatch of h-BN and the substrates (Fig. 13a and b) [114,115]. On Rh(1 1 1), a highly corrugated h-BN was formed (so called boron nitride nanomesh), which consisted of *pore* regions with strong interaction separated by *wire* regions with weaker interaction [115,116]. Researchers found that molecules selectively adsorbed in the pore regions. For example, metal free phthalocyanine (H_2Pc) and CuPc showed selective molecular adsorption in the pore regions of h-BN/Rh(1 1 1) [116]. Moreover, it has been demonstrated that the molecular orientations are aligned (Fig. 13c and d) [116]. Similarly, h-BN/Ru(0001) also showed strong adsorption selectivity in the pore regions for Fe_4H compounds (Fig. 13e and f) [117]. The selective adsorption in the pore regions is a general phenomenon, which has been observed, for example, in CoPc on h-BN/Ir(1 1 1) [118], and porphine and tetracyanoquinodimethane (TCNQ) on h-BN/Cu(1 1 1) [119]. Interestingly, different molecular charging states were observed depending on the adsorption site in the h-BN moiré [118].

Inorganic nanomaterials assembled on graphene and h-BN moiré substrates

Moiré patterns formed between 2D materials and epitaxial substrates have also been considered as good templates for fabricating periodic arrays of inorganic nanomaterials (especially metal nanocrystals) as shown in Fig. 14. Various metals have been deposited from the vapor phase on the moiré patterns, and specific locations in the moiré supercell provided nucleation sites for the deposited metal atoms to aggregate into regular island distributions. The most notable results were obtained for the graphene moiré structures on Ir(1 1 1), as shown by the Michely group, where they successfully fabricated periodic arrays of Ir, Pt, W, Re, Co, Eu, Au, AuIr, and FeIr nanoislands [120–126]. The graphene moiré structures on Ru(0001) also provided similar (but less periodic) results with Pt, Rh, Pd, Co, and Au nanoislands [127–129]. Graphene on SiC(0001), which is believed to have weak interaction, is normally used as a model substrate to study the interaction between graphene (uninfluenced by its substrate) and metals, as discussed in the previous section; however, the moiré structure still exists and can be used for fabricating periodic arrays of Cs nanoislands [130,131]. The h-BN moiré structures on Rh(1 1 1) or Ru(0001) can also generate periodic arrays of metal nanoislands [132–136], but their periodicity is generally weaker than that on the graphene moiré structures.

Applications of the self-organized growth on 2D materials

The self-organized growth and self-assembly on 2D materials discussed in this review are essentially one of the bottom-up synthesis methods, which have been expected to show huge impact from the early stage of nanotechnology [137]. Although the potential of bottom-up synthesis on a surface cannot be undermined, its practical applications in the current scenario might be questionable. In this section, we focus on reviewing examples that currently present the realistic applications of the self-organized and self-assembled nanomaterials on 2D materials.

Nanofabrication with controlled crystallographic orientations

Combining the self-organized growth on 2D materials with top-down fabrication methods provides us a new class of fabrication technique for nanoscale devices. One typical example is the van der Waals heterostructures with controlled crystallographic

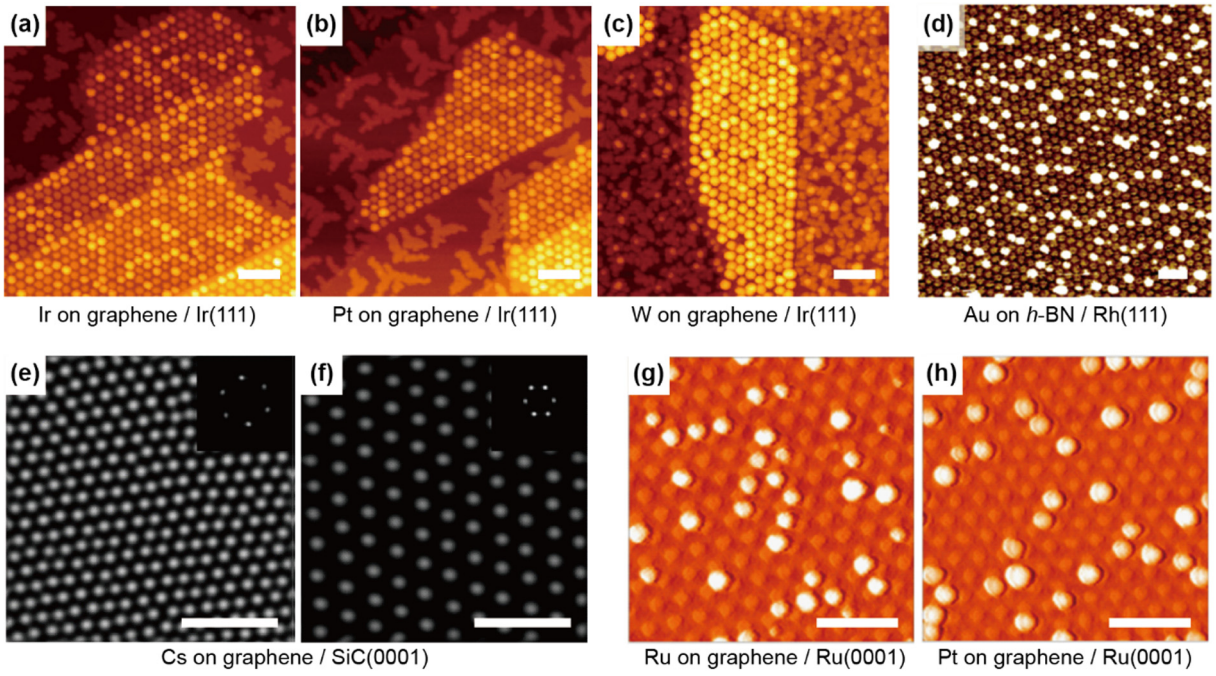

Fig. 14. Metals self-organized on 2D material moiré. (a–c) STM images of Ir (a), Pt (b), and W (c) nanostructures deposited on graphene/Ir(1 1 1) moiré. (d) STM image of Au nanostructures deposited on h-BN/Rh(1 1 1) moiré. (e,f) STM images of Cs nanostructures deposited on single (e) and double (f) layered graphene/SiC(0001) moiré. (g,h) STM images of Ru (g) and Pt (h) nanostructures on graphene/Ru(0001) moiré. All scale bars are 10 nm. (a)–(c) [120], Copyright © 2009 IOP Publishing. (d) [132], Copyright © 2017, Elsevier B.V. (e) and (f) [130]. (g) and (h) [136], Copyright © 2013, AIP Publishing LLC.

Please cite this article in press as: J. Yang et al., Self-organized growth and self-assembly of nanostructures on 2D materials, FlatChem (2017), http://dx.doi.org/10.1016/j.flatc.2017.07.004

orientations. In some of van der Waals heterostructures, the crystallographic alignment between the stacked 2D materials had unprecedented synergetic effects on resonant tunneling and electronic band structures. It is worth noting that the self-organized growth is one of the ideal methods to achieve crystallographic alignment. For example, the CVD grown atomically thin MoS_2/WSe_2/graphene and WSe_2/MoS_2/graphene heterostructures can act as resonant tunnel diodes [101]. Most strikingly, they show negative differential resistance even at room temperature, which has been known to occur at liquid nitrogen temperature for the conventional mechanically stacked heterostructures. This unique phenomenon was attributed to the optimal coupling of two 2D crystals, which originated from a strict rotational alignment between the self-aligned 2D materials. Relative orientation between the MoS_2 layer and WSe_2 layer is only ~2°, whereas mechanically transferred MoS_2/WSe_2 heterostructures exhibit a broad distribution in their relative crystal orientation. Furthermore, the self-aligned 2D/2D materials with a precise crystal alignment provide excellent model systems to study the superlattice effects such as the superlattice Dirac points and Hofstadter butterfly in high magnetic fields. The self-aligned graphene on h-BN crystals showed a clean superlattice, exhibiting Hofstadter butterfly features at a low magnetic field of 6.4 T, which had not been observed previously [138]. In addition to the 2D/2D material structures, inorganic materials self-aligned on 2D materials also allow us to fabricate nanostructures with controlled crystallographic orientations. Graphene nanoribbons with zigzag-edged directions, which can be important components in spintronic devices, were fabricated with AuCN nanowires synthesized on graphene [62]. The AuCN nanowires preferentially aligned along the zigzag-lattice directions of the underlying graphene and were used as a mask for graphene etching, thereby enabling the control of crystallographic orientations of the resulting graphene nanoribbons.

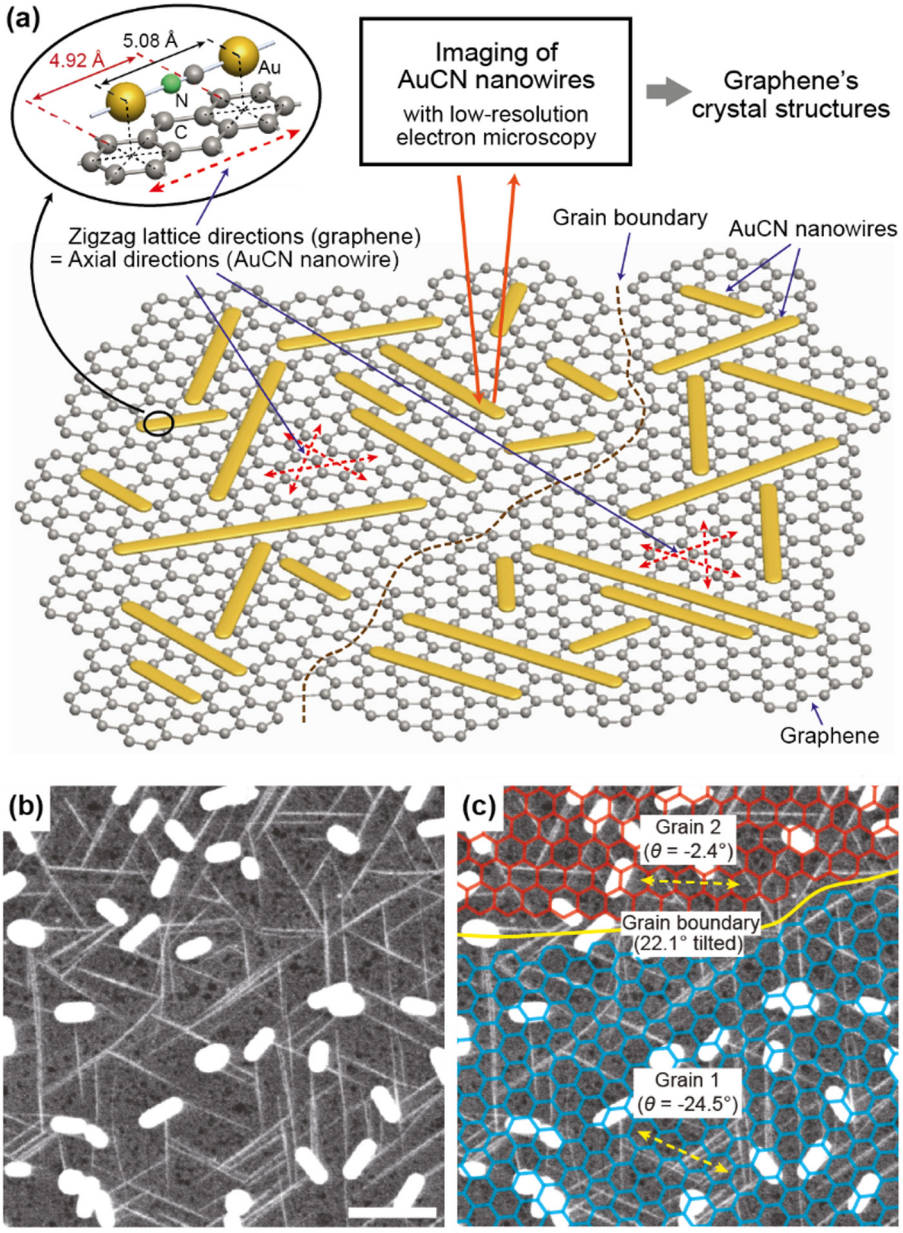

Fig. 15. Facile identification of crystal structures of polycrystalline 2D materials based on self-aligned nanomaterials. (a) Conceptual illustration of the identification method. (b) SEM image of the AuCN nanowires on graphene. The scale bar is 200 nm. (c) The same SEM image of (b) with an overlay of the pseudolattice structures of graphene. The red and blue color maps represent different grains with relatively tilted lattice orientations [63]. Copyright © 2017, American Chemical Society.

Please cite this article in press as: J. Yang et al., Self-organized growth and self-assembly of nanostructures on 2D materials, FlatChem (2017), http://dx.doi.org/10.1016/j.flatc.2017.07.004

In case of organic molecules, self-assembly on 2D materials is one of the excellent ways to fabricate high-quality organic crystals. Large-grain organic crystals (single-crystals in some works) with a high-quality interface and a low density of charge traps, which are the key factors for high-performance organic electronics, can be achieved using 2D materials as the growth template. Various organic devices such as organic photovoltaics (OPVs), organic field effect transistors (OTFTs), and organic light emitting diodes (OLEDs) have been demonstrated using organic assemblies on 2D materials. Particularly, graphene can serve as transparent, functional electrodes for OTFTs, OPVs, and OLEDs. h-BN, on the other hand, can serve as an excellent dielectric interface template for OTFTs. For example, researchers have demonstrated organic/graphene vertical transistors using various small organic molecules [41]. Similarly, using an organic molecular assembly on a mechanically exfoliated h-BN, researchers have fabricated high-performance organic transistors [41,47]. Moreover, very recently, an organic assembly on CVD-grown h-BN was utilized for a similar application, which opens up the possibility of using them in large-area electronics applications [50].

Crystallographic mapping of 2D materials

The self-organized growth and self-assembly were also applied for facile identification of crystal structures (crystal orientation and grain boundary) of 2D materials. In the previous sections, we discussed various examples where the nanomaterials grown on 2D materials aligned their internal or external structures along certain crystal orientations of the underlying 2D materials. These phenomena can be described as the "transfer" and/or "amplification" of the crystallographic (atomic) structures of the 2D materials to the nanomaterials; thus, the determination of nanomaterial structure (which is relatively simple) enables the crystallographic mapping of the host 2D materials. As shown in Fig. 15, the nanomaterial orientations identified by facile imaging tools directly represent the crystal orientations of the underlying 2D materials, and changes in the nanomaterial orientations indicate tilt grain boundaries in the 2D materials. It is worth noting that the atomic resolution imaging tools such as TEM [139,140] and STM (scanning tunneling microscopy) [125,141,142] that have traditionally been used for the crystallographic mapping of 2D materials involve complex sample preparation and are time-consuming processes.

The present idea was initially suggested (but very briefly mentioned) in a previous work [40] where phosphonic acids aligned on graphene were observed using AFM (atomic force microscopy). It was later expanded to the crystallographic mapping of MoS_2 [54], where AFM might not be suitable for large-scale imaging. Using liquid crystal has also enabled crystallographic mapping of 2D materials by optical microscopy [143]. Graphene was the first target to be analyzed by imaging the birefringence of liquid crystals using polarized optical microscopy (POM) [143,144], following which other 2D materials such as MoS_2, $MoSe_2$, and WSe_2 were also analyzed [145,146]. This method (so called liquid crystalline texture method) has various advantages such as facile and large-scale imaging and simple deposition and removal of liquid crystals. However, the method cannot measure the absolute values of crystallographic orientations of 2D materials because optical birefringence is dependent on the thickness of the liquid crystal layers [143]. We also note that there is a debate about whether the liquid crystalline texture method reveals the grain boundaries of the 2D materials or those of the underlying substrates [147].

Inorganic materials can be more efficient for the crystallographic mapping of 2D materials because scanning electron microscopy (SEM) can be used for the imaging of inorganic materials. SEM-based identification of crystal directions and grain boundaries in polycrystalline graphene was first suggested and verified using AuCN nanowires [62]. Then, a similar method based on MoS_2 nanotriangles enabled the crystallographic mapping of graphene and WS_2 [97]. Recently, a statistical method for improving the accuracy of measurement was suggested, and a simple removal method for AuCN nanowires without damaging the graphene was verified [63], which furthered this idea towards practical applications. The final goal of this idea might be the identification of crystal structures including the "absolute crystal orientations" of 2D materials via "optical microscopy" of epitaxial nanomaterials that can be "simply deposited and removed".

Conclusion

In this review article, we have discussed the self-organized growth and self-assembly on 2D materials. A wide range of materials, including organic molecules, inorganic nanomaterials, and 2D materials, have been successfully grown on the atomically flat surfaces of 2D materials. Strong van der Waals interaction between the grown nanostructures and 2D materials controls the self-organization process, which finally results in the self-alignment of the relative orientation between the grown nanomaterials and 2D substrates. Regardless of the growing materials and growth methods, the self-alignment behavior is found to be universal, and can be attributed to the minimization of interfacial energy during the self-organization process. The self-alignment behavior can be used for nanofabrication by creating heterostructures with fixed relative crystal orientations and clean interfaces, thus resulting in novel phenomena and superior electrical properties. Moreover, the self-organized growth is useful for the direct determination of grain structures of 2D materials, which significantly influences the properties of the 2D materials.

Acknowledgements

This work was supported by the Research Center Program of Institute for Basic Science (IBS-R006-D1) in Korea. J. P. acknowledges support by the National Research Foundation of Korea (NRF) grant funded by the Korea government (MSIP) (No. NRF-2017R1A5A1015365). W.C.L. and Kihwan K. gratefully acknowledge support from the Basic Science Research Program and the Convergence Technology Development Program for Bionic Arm through the National Research Foundation of Korea (NRF) funded by the Ministry of Science, ICT & Future Planning (2016R1C1B1014940 and 2015M3C1B2052811). Y.L. and Kwanpyo K. gratefully acknowledge support from the Basic Science Research Program through the National Research Foundation of Korea (NRF) funded by the Ministry of Education (NRF-2016R1D1A1B03934008). Kwanpyo K. also acknowledges support from the 2015 Research Fund (1.150118.01) of UNIST.

References

[1] A.K. Geim, I.V. Grigorieva, Nature 499 (2013) 419–425.
[2] K.S. Novoselov, A. Mishchenko, A. Carvalho, A.H. Castro Neto, Science 353 (2016), aac9439.
[3] Y. Liu, N.O. Weiss, X. Duan, H.-C. Cheng, Y. Huang, X. Duan, Nat. Rev. Mater. 1 (2016) 16042.
[4] K. Kim, S. Coh, L.Z. Tan, W. Regan, J.M. Yuk, E. Chatterjee, M.F. Crommie, M.L. Cohen, S.G. Louie, A. Zettl, Phys. Rev. Lett. 108 (2012) 246103.
[5] M.K. Choi, I. Park, D.C. Kim, E. Joh, O.K. Park, J. Kim, M. Kim, C. Choi, J. Yang, K. W. Cho, J.-H. Hwang, J.-M. Nam, T. Hyeon, J.H. Kim, D.-H. Kim, Adv. Funct. Mater. 25 (2015) 7109–7118.
[6] Y. Zhang, T.-T. Tang, C. Girit, Z. Hao, M.C. Martin, A. Zettl, M.F. Crommie, Y.R. Shen, F. Wang, Nature 459 (2009) 820–823.
[7] A. Luican, G. Li, A. Reina, J. Kong, R.R. Nair, K.S. Novoselov, A.K. Geim, E.Y. Andrei, Phys. Rev. Lett. 106 (2011) 126802.
[8] M. Yankowitz, J. Xue, D. Cormode, J.D. Sanchez-Yamagishi, K. Watanabe, T. Taniguchi, P. Jarillo-Herrero, P. Jacquod, B.J. LeRoy, Nat. Phys. 8 (2012) 382–386.

[9] C.R. Woods, L. Britnell, A. Eckmann, R.S. Ma, J.C. Lu, H.M. Guo, X. Lin, G.L. Yu, Y. Cao, R.V. Gorbachev, A.V. Kretinin, J. Park, L.A. Ponomarenko, M.I. Katsnelson, Y.N. Gornostyrev, K. Watanabe, T. Taniguchi, C. Casiraghi, H.J. Gao, A.K. Geim, K.S. Novoselov, Nat. Phys. 10 (2014) 451–456.
[10] V. Georgakilas, J.N. Tiwari, K.C. Kemp, J.A. Perman, A.B. Bourlinos, K.S. Kim, R. Zboril, Chem. Rev. 116 (2016) 5464–5519.
[11] Q. Quan, X. Lin, N. Zhang, Y.-J. Xu, Nanoscale 9 (2017) 2398–2416.
[12] Z. Li, S. Wu, W. Lv, J.-J. Shao, F. Kang, Q.-H. Yang, Small 12 (2016) 2674–2688.
[13] X. Huang, X. Qi, F. Boey, H. Zhang, Chem. Soc. Rev. 41 (2012) 666–686.
[14] D.E. Hooks, T. Fritz, M.D. Ward, Adv. Mater. 13 (2001) 227–241.
[15] J.M. MacLeod, F. Rosei, Small 10 (2013) 1038–1049.
[16] G. Neri, N. Micale, A. Scala, E. Fazio, A. Mazzaglia, P.G. Mineo, M. Montesi, S. Panseri, A. Tampieri, G. Grassi, A. Piperno, FlatChem 1 (2017) 34–41.
[17] M. Marcia, A. Hirsch, F. Hauke, FlatChem 1 (2017) 89–103.
[18] Y. Zhao, Q. Wu, Q. Chen, J. Wang, J. Phys. Chem. Lett. 6 (2015) 4518–4524.
[19] S. De Feyter, F.C. De Schryver, Chem. Soc. Rev. 32 (2003) 139–150.
[20] Y. Okawa, M. Aono, J. Chem. Phys. 115 (2001) 2317–2322.
[21] B. Grévin, P. Rannou, R. Payerne, A. Pron, J.P. Travers, Adv. Mater. 15 (2003) 881–884.
[22] W. Chen, H. Huang, A. Thye, S. Wee, Chem. Commun. 14 (2008) 4276–4278.
[23] J. Götzen, D. Käfer, C. Wöll, G. Witte, Phys. Rev. B 81 (2010) 085440.
[24] L.K. Thomas, A. Kühnle, S. Rode, U. Beginn, M. Reichling, J. Phys. Chem. C 114 (2010) 18919–18924.
[25] F. Zhang, H.-N. Du, Z.-X. Zhang, L.-N. Ji, H.-T. Li, L. Tang, H.-B. Wang, C.-H. Fan, H.-J. Xu, Y. Zhang, J. Hu, H.-Y. Hu, J.-H. He, Angew. Chem. Int. Ed. 45 (2006) 3611–3613.
[26] J. Wintterlin, M.L. Bocquet, Surf. Sci. 603 (2009) 1841–1852.
[27] J. Cho, J. Smerdon, L. Gao, Ö. Süzer, J.R. Guest, N.P. Guisinger, Nano Lett. 12 (2012) 3018–3024.
[28] M. Švec, P. Merino, Y.J. Dappe, C. González, E. Abad, P. Jelínek, J.A. Martín-Gago, Phys. Rev. B 86 (2012) 121407.
[29] M. Jung, D. Shin, S.-D. Sohn, S.-Y. Kwon, N. Park, H.-J. Shin, Nanoscale 6 (2014) 11835–11841.
[30] Q.H. Wang, M.C. Hersam, Nat. Chem. 1 (2009) 206–211.
[31] B. Li, K. Tahara, J. Adisoejoso, W. Vanderlinden, K.S. Mali, S. De Gendt, Y. Tobe, S. De Feyter, ACS Nano 7 (2013) 10764–10772.
[32] P. Järvinen, S.K. Hämäläinen, M. Ijäs, A. Harju, P. Liljeroth, J. Phys. Chem. C 118 (2014) 13320–13325.
[33] X. Li, W. Cai, J. An, S. Kim, J. Nah, D. Yang, R. Piner, A. Velamakanni, I. Jung, E. Tutuc, S.K. Banerjee, L. Colombo, R.S. Ruoff, Science 324 (2009) 1312–1314.
[34] W.H. Lee, J. Park, S.H. Sim, S. Lim, K.S. Kim, B.H. Hong, K. Cho, J. Am. Chem. Soc. 133 (2011) 4447–4454.
[35] K. Kim, E.J.G. Santos, T.H. Lee, Y. Nishi, Z. Bao, Small 11 (2015) 2037–2043.
[36] M. Chhikara, E. Pavlica, A. Matković, A. Beltaos, R. Gajić, G. Bratina, Carbon 69 (2014) 162–168.
[37] B. Frank, H.H. Henrik, B.K. Mikkel, J.B. Timothy, S. Rong, P. Jürgen, S. Manuela, B. Peter, Nanotechnology 25 (2014) 035602.
[38] I. Salzmann, A. Moser, M. Oehzelt, T. Breuer, X. Feng, Z.-Y. Juang, D. Nabok, R. G. Della Valle, S. Duhm, G. Heimel, A. Brillante, E. Venuti, I. Bilotti, C. Christodoulou, J. Frisch, P. Puschnig, C. Draxl, G. Witte, K. Müllen, N. Koch, ACS Nano 6 (2012) 10874–10883.
[39] K. Kim, T.H. Lee, E.J.G. Santos, P.S. Jo, A. Salleo, Y. Nishi, Z. Bao, ACS Nano 9 (2015) 5922–5928.
[40] M.C. Prado, R. Nascimento, L.G. Moura, M.J.S. Matos, M.S.C. Mazzoni, L.G. Cancado, H. Chacham, B.R.A. Neves, ACS Nano 5 (2011) 394–398.
[41] D. He, Y. Zhang, Q. Wu, R. Xu, H. Nan, J. Liu, J. Yao, Z. Wang, S. Yuan, Y. Li, Z. Ni, L. He, F. Miao, F. Song, H. Xu, K. Watanabe, T. Taniguchi, J.-B. Xu, Y. Shi, J. Wang, X. Wang, Nat. Commun. 5 (2014) 5162.
[42] Y.-J. Yu, G.-H. Lee, J.I. Choi, Y.S. Shim, C.-H. Lee, S.J. Kang, S. Lee, K.T. Rim, G.W. Flynn, J. Hone, Y.-H. Kim, P. Kim, C. Nuckolls, S. Ahn, Adv. Mater. 29 (2016) 1603925.
[43] C. Huang, M. He, D. Liu, X. Sun, B. Gao, J. Phys. Chem. C 120 (2016) 17564–17569.
[44] P. Järvinen, S.K. Hämäläinen, K. Banerjee, P. Häkkinen, M. Ijäs, A. Harju, P. Liljeroth, Nano Lett. 13 (2013) 3199–3204.
[45] M. Gulde, S. Schweda, G. Storeck, M. Maiti, H.K. Yu, A.M. Wodtke, S. Schäfer, C. Ropers, Science 345 (2014) 200–204.
[46] J.W. Colson, A.R. Woll, A. Mukherjee, M.P. Levendorf, Science 332 (2011) 228–231.
[47] C.-H. Lee, T. Schiros, E.J.G. Santos, B. Kim, K.G. Yager, S.J. Kang, S. Lee, J. Yu, K. Watanabe, T. Taniguchi, J. Hone, E. Kaxiras, C. Nuckolls, P. Kim, Adv. Mater. 26 (2014) 2812–2817.
[48] A. Matković, J. Genser, D. Lüftner, M. Kratzer, R. Gajić, P. Puschnig, C. Teichert, Sci. Rep. 6 (2016) 38519.
[49] Y. Zhang, J. Qiao, S. Gao, F. Hu, D. He, B. Wu, Z. Yang, B. Xu, Y. Li, Y. Shi, W. Ji, P. Wang, X. Wang, M. Xiao, H. Xu, J.-B. Xu, X. Wang, Phys. Rev. Lett. 116 (2016) 016602.
[50] T.H. Lee, K. Kim, G. Kim, H.J. Park, D. Scullion, L. Shaw, M.-G. Kim, X. Gu, W.-G. Bae, E.J.G. Santos, Z. Lee, H.S. Shin, Y. Nishi, Z. Bao, Chem. Mater. 29 (2017) 2341–2347.
[51] C. Ludwig, R. Strohmaier, J. Petersen, B. Gompf, W. Eisenmenger, J. Vac. Sci. Technol. B 12 (1994) 1963–1966.
[52] G.E. Collins, V.S. Williams, L.K. Chau, K.W. Nebesny, C. England, P.A. Lee, T. Lowe, Q. Fernando, N.R. Armstrong, Synth. Met. 54 (1993) 351–362.
[53] R. Giridharagopal, K.F. Kelly, ACS Nano 2 (2008) 1571–1580.
[54] M.C. Prado, R. Nascimento, B.E.N. Faria, M.J.S. Matos, H. Chacham, B.R.A. Neves, Nanotechnology 26 (2015) 475702.
[55] Y.J. Zheng, Y.L. Huang, Y. Chen, W. Zhao, G. Eda, C.D. Spataru, W. Zhang, Y.-H. Chang, L.-J. Li, D. Chi, S.Y. Quek, A.T.S. Wee, ACS Nano 10 (2016) 2476–2484.
[56] A. Koma, Thin Solid Films 216 (1992) 72–76.
[57] W.H. Dang, H.L. Peng, H. Li, P. Wang, Z.F. Liu, Nano Lett. 10 (2010) 2870–2876.
[58] Y.J. Hong, J.W. Yang, W.H. Lee, R.S. Ruoff, K.S. Kim, T. Fukui, Adv. Mater. 25 (2013) 6847–6853.
[59] Y.J. Hong, T. Fukui, ACS Nano 5 (2011) 7576–7584.
[60] Y.J. Hong, W.H. Lee, Y.P. Wu, R.S. Ruoff, T. Fukui, Nano Lett. 12 (2012) 1431–1436.
[61] Y. Kim, S.S. Cruz, K. Lee, B.O. Alawode, C. Choi, Y. Song, J.M. Johnson, C. Heidelberger, W. Kong, S. Choi, K. Qiao, I. Almansouri, E.A. Fitzgerald, J. Kong, A.M. Kolpak, J. Hwang, J. Kim, Nature 544 (2017) 340–343.
[62] W.C. Lee, K. Kim, J. Park, J. Koo, H.Y. Jeong, H. Lee, D.A. Weitz, A. Zettl, S. Takeuchi, Nat. Nanotechnol. 10 (2015) 423–428.
[63] J. Kim, K. Lim, Y. Lee, J. Kim, K. Kim, J. Park, K. Kim, W.C. Lee, J. Phys. Chem. Lett. 8 (2017) 1302–1309.
[64] H.Y. Ma, H.T. Wang, P.C. Burns, B.K. McNamara, E.C. Buck, C.Z. Na, J. Nucl. Mater. 475 (2016) 113–122.
[65] X.J. Liu, C.Z. Wang, M. Hupalo, H.Q. Lin, K.M. Ho, M.C. Tringides, Crystals 3 (2013) 79–111.
[66] X.J. Liu, Y. Han, J.W. Evans, A.K. Engstfeld, R.J. Behm, M.C. Tringides, M. Hupalo, H.Q. Lin, L. Huang, K.M. Ho, D. Appy, P.A. Thiel, C.Z. Wang, Prog. Surf. Sci. 90 (2015) 397–443.
[67] P.F. Xu, L. Dong, M. Neek-Amal, M.L. Ackerman, J.H. Yu, S.D. Barber, J.K. Schoelz, D.J. Qi, F.F. Xu, P.M. Thibado, F.M. Peeters, ACS Nano 8 (2014) 2697–2703.
[68] X.J. Liu, C.Z. Wang, M. Hupalo, Y.X. Yao, M.C. Tringides, W.C. Lu, K.M. Ho, Phys. Rev. B 82 (2010) 245408.
[69] M. Hupalo, X.J. Liu, C.Z. Wang, W.C. Lu, Y.X. Yao, K.M. Ho, M.C. Tringides, Adv. Mater. 23 (2011) 2082–2087.
[70] M. Hupalo, S. Binz, M.C. Tringides, J. Phys. Condens. Matter. 23 (2011) 045005.
[71] X.J. Liu, C.Z. Wang, M. Hupalo, W.C. Lu, M.C. Tringides, Y.X. Yao, K.M. Ho, Phys. Chem. Chem. Phys. 14 (2012) 9157–9166.
[72] S.M. Binz, M. Hupalo, X.J. Liu, C.Z. Wang, W.C. Lu, P.A. Thiel, K.M. Ho, E.H. Conrad, M.C. Tringides, Phys. Rev. Lett. 109 (2012) 026103.
[73] X.J. Liu, M. Hupalo, C.Z. Wang, W.C. Lu, P.A. Thiel, K.M. Ho, M.C. Tringides, Phys. Rev. B 86 (2012) 081414.
[74] E.L. Evans, O.P. Bahl, J.M. Thomas, Carbon 5 (1967) 587–589.
[75] H.Q. Zhou, F. Yu, M.J. Chen, C.Y. Qiu, H.C. Yang, G. Wang, T. Yu, L.F. Sun, Carbon 52 (2013) 379–387.
[76] Z.T. Luo, L.A. Somers, Y.P. Dan, T. Ly, N.J. Kybert, E.J. Mele, A.T.C. Johnson, Nano Lett. 10 (2010) 777–781.
[77] D. Kiriya, Y.Z. Zhou, C. Nelson, M. Hettick, S.R. Madhvapathy, K. Chen, P.D. Zhao, M. Tosun, A.M. Minor, D.C. Chrzan, A. Javey, Adv. Funct. Mater. 25 (2015) 6257–6264.
[78] X. Huang, X.Z. Zhou, S.X. Wu, Y.Y. Wei, X.Y. Qi, J. Zhang, F. Boey, H. Zhang, Small 6 (2010) 513–516.
[79] J.M.P. Alaboson, C.H. Sham, S. Kewalramani, J.D. Emery, J.E. Johns, A. Deshpande, T.Y. Chien, M.J. Bedzyk, J.W. Elam, M.J. Pellin, M.C. Hersam, Nano Lett. 13 (2013) 5763–5770.
[80] J.M.P. Alaboson, Q.H. Wang, J.D. Emery, A.L. Lipson, M.J. Bedzyk, J.W. Elam, M. J. Pellin, M.C. Hersam, ACS Nano 5 (2011) 5223–5232.
[81] X. Huang, S. Li, Y. Huang, S. Wu, X. Zhou, S. Li, C.L. Gan, F. Boey, C.A. Mirkin, H. Zhang, Nat. Commun. 2 (2011) 292.
[82] Z. Liu, L. Song, S. Zhao, J. Huang, L. Ma, J. Zhang, J. Lou, P.M. Ajayan, Nano Lett. 11 (2011) 2032–2037.
[83] X. Ding, G. Ding, X. Xie, F. Huang, M. Jiang, Carbon 49 (2011) 2522–2525.
[84] W. Gannett, W. Regan, K. Watanabe, T. Taniguchi, M.F. Crommie, A. Zettl, Appl. Phys. Lett. 98 (2011) 242105.
[85] W. Yang, G. Chen, Z. Shi, C.C. Liu, L. Zhang, G. Xie, M. Cheng, D. Wang, R. Yang, D. Shi, Nat. Mater. 12 (2013) 792–797.
[86] A. Yan, J. Velasco, S. Kahn, K. Watanabe, T. Taniguchi, F. Wang, M.F. Crommie, A. Zettl, Nano Lett. 15 (2015) 6324–6331.
[87] S. Wang, X. Wang, J.H. Warner, ACS Nano 9 (2015) 5246–5254.
[88] Y. Shi, W. Zhou, A.-Y. Lu, W. Fang, Y.-H. Lee, A.L. Hsu, S.M. Kim, K.K. Kim, H.Y. Yang, L.-J. Li, J.-C. Idrobo, J. Kong, Nano Lett. 12 (2012) 2784–2791.
[89] Y.C. Lin, N. Lu, N. Perea-Lopez, J. Li, Z. Lin, X. Peng, C.H. Lee, C. Sun, L. Calderin,, P.N. Browning, M.S. Bresnehan, M.J. Kim, T.S. Mayer, M. Terrones, J.A. Robinson, ACS Nano 8 (2014) 3715–3723.
[90] X. Li, L. Basile, B. Huang, C. Ma, J. Lee, I.V. Vlassiouk, A.A. Puretzky, M.-W. Lin, M. Yoon, M. Chi, J.C. Idrobo, C.M. Rouleau, B.G. Sumpter, D.B. Geohegan, K. Xiao, ACS Nano 9 (2015) 8078–8088.
[91] C.R. Dean, A.F. Young, I. Meric, C. Lee, L. Wang, S. Sorgenfrei, K. Watanabe, T. Taniguchi, P. Kim, K.L. Shepard, J. Hone, Nat. Nanotechnol. 5 (2010) 722–726.
[92] J.H. Chen, C. Jang, S. Xiao, M. Ishigami, M.S. Fuhrer, Nat. Nanotechnol. 3 (2008) 206–209.
[93] J. Martin, N. Akerman, G. Ulbricht, T. Lohmann, J.H. Smet, K. von Klitzing, A. Yacoby, Nat. Phys. 4 (2008) 144–148.
[94] A. Koma, J. Cryst. Growth 201/202 (1999) 236–241.
[95] S. Najmaei, Z. Liu, W. Zhou, X. Zou, G. Shi, S. Lei, B.I. Yakobson, J.C. Idrobo, P.M. Ajayan, J. Lou, Nat. Mater. 12 (2013) 754–759.
[96] A.M. Van der Zande, P.Y. Huang, D.A. Chenet, T.C. Berkelbach, Y. You, G.H. Lee, T.F. Heinz, D.R. Reichman, D.A. Muller, J.C. Hone, Nat. Mater. 12 (2013) 554–561.

Please cite this article in press as: J. Yang et al., Self-organized growth and self-assembly of nanostructures on 2D materials, FlatChem (2017), http://dx.doi.org/10.1016/j.flatc.2017.07.004

[97] H. Ago, S. Fukamachi, H. Endo, P. Solís-Fernández, R. Mohamad Yunus, Y. Uchida, V. Panchal, O. Kazakova, M. Tsuji, ACS Nano 10 (2016) 3233–3240.
[98] K.K. Kim, A. Reina, Y. Shi, H. Park, L.-J. Li, Y.H. Lee, J. Kong, Nanotechnology 21 (2010) 285205.
[99] Y. Gong, J. Lin, X. Wang, G. Shi, S. Lei, Z. Lin, X. Zou, G. Ye, R. Vajtai, B.I. Yakobson, H. Terrones, M. Terrones, Beng K. Tay, J. Lou, S.T. Pantelides, Z. Liu, W. Zhou, P.M. Ajayan, Nat. Mater. 13 (2014) 1135–1142.
[100] X. Duan, C. Wang, J.C. Shaw, R. Cheng, Y. Chen, H. Li, X. Wu, Y. Tang, Q. Zhang, A. Pan, J. Jiang, R. Yu, Y. Huang, X. Duan, Nat. Nanotechnol. 9 (2014) 1024–1030.
[101] Y.-C. Lin, R.K. Ghosh, R. Addou, N. Lu, S.M. Eichfeld, H. Zhu, M.-Y. Li, X. Peng, M.J. Kim, L.-J. Li, R.M. Wallace, S. Datta, J.A. Robinson, Nat. Commun. 6 (2015) 7311.
[102] Y.-C. Lin, C.-Y.S. Chang, R.K. Ghosh, J. Li, H. Zhu, R. Addou, B. Diaconescu, T. Ohta, X. Peng, N. Lu, M.J. Kim, J.T. Robinson, R.M. Wallace, T.S. Mayer, S. Datta, L.-J. Li, J.A. Robinson, Nano Lett. 14 (2014) 6936–6941.
[103] M. Cattelan, B. Markman, G. Lucchini, P.K. Das, I. Vobornik, J.A. Robinson, S. Agnoli, G. Granozzi, Chem. Mater. 27 (2015) 4105–4113.
[104] J.H. Yu, H.R. Lee, S.S. Hong, D. Kong, H.-W. Lee, H. Wang, F. Xiong, S. Wang, Y. Cui, Nano Lett. 15 (2015) 1031–1035.
[105] Z. Xu, R. Zheng, A. Khanaki, Z. Zuo, J. Liu, Appl. Phys. Lett. 107 (2015) 213103.
[106] H.C. Diaz, R. Chaghi, Y. Ma, M. Batzill, 2D Mater. 2 (2015) 044010.
[107] E. Xenogiannopoulou, P. Tsipas, K.E. Aretouli, D. Tsoutsou, S.A. Giamini, C. Bazioti, G.P. Dimitrakopulos, P. Komninou, S. Brems, C. Huyghebaert, I.P. Radu, A. Dimoulas, Nanoscale 7 (2015) 7896–7905.
[108] J. Lu, P.S.E. Yeo, Y. Zheng, Z. Yang, Q. Bao, C.K. Gan, K.P. Loh, ACS Nano 6 (2012) 944–950.
[109] G. Li, H.T. Zhou, L.D. Pan, Y. Zhang, J.H. Mao, Q. Zou, H.M. Guo, Y.L. Wang, S.X. Du, H.-J. Gao, Appl. Phys. Lett. 100 (2012) 013304.
[110] H.G. Zhang, J.T. Sun, T. Low, L.Z. Zhang, Y. Pan, Q. Liu, J.H. Mao, H.T. Zhou, H.M. Guo, S.X. Du, F. Guinea, H.-J. Gao, Phys. Rev. B 84 (2011) 245436.
[111] H. Zhou, L. Zhang, J. Mao, G. Li, Y. Zhang, Y. Wang, S. Du, W.A. Hofer, H.-J. Gao, Nano Res. 6 (2013) 131–137.
[112] J. Mao, H. Zhang, Y. Jiang, Y. Pan, M. Gao, W. Xiao, H.-J. Gao, J. Am. Chem. Soc. 131 (2009) 14136–14137.
[113] D. Maccariello, M. Garnica, M.A. Niño, C. Navío, P. Perna, S. Barja, A.L. Vázquez de Parga, R. Miranda, Chem. Mater. 26 (2014) 2883–2890.
[114] M. Corso, W. Auwärter, M. Muntwiler, A. Tamai, T. Greber, J. Osterwalder, Science 303 (2004) 217–220.
[115] S. Berner, M. Corso, R. Widmer, O. Groening, R. Laskowski, P. Blaha, K. Schwarz, A. Goriachko, H. Over, S. Gsell, M. Schreck, H. Sachdev, T. Greber, J. Osterwalder, Angew. Chem. Int. Ed. 46 (2007) 5115–5119.
[116] M. Iannuzzi, F. Tran, R. Widmer, T. Dienel, K. Radican, Y. Ding, J. Hutter, O. Groning, Phys. Chem. Chem. Phys. 16 (2014) 12374–12384.
[117] P. Erler, P. Schmitt, N. Barth, A. Irmler, S. Bouvron, T. Huhn, U. Groth, F. Pauly, L. Gragnaniello, M. Fonin, Nano Lett. 15 (2015) 4546–4552.
[118] F. Schulz, R. Drost, S.K. Hämäläinen, P. Liljeroth, ACS Nano 7 (2013) 11121–11128.
[119] S. Joshi, F. Bischoff, R. Koitz, D. Ecija, K. Seufert, A.P. Seitsonen, J. Hutter, K. Diller, J.I. Urgel, H. Sachdev, J.V. Barth, W. Auwärter, ACS Nano 8 (2014) 430–442.
[120] A.T. N'Diaye, T. Gerber, C. Busse, J. Myslivecek, J. Coraux, T. Michely, New J. Phys. 11 (2009) 103045.
[121] C. Vo-Van, S. Schumacher, J. Coraux, V. Sessi, O. Fruchart, N.B. Brookes, P. Ohresser, T. Michely, Appl. Phys. Lett. 99 (2011) 142504.
[122] C. Vo-Van, Z. Kassir-Bodon, H. Yang, J. Coraux, J. Vogel, S. Pizzini, P. Bayle-Guillemaud, M. Chshiev, L. Ranno, V. Guisset, P. David, V. Salvador, O. Fruchart, New J. Phys. 12 (2010) 103040.
[123] D.F. Forster, T.O. Wehling, S. Schumacher, A. Rosch, T. Michely, New J. Phys. 14 (2012) 023022.
[124] J. Coraux, A.T. N'Diaye, M. Engler, C. Busse, D. Wall, N. Buckanie, F. Heringdorf, R. van Gastel, B. Poelsema, T. Michely, New J. Phys. 11 (2009) 023006.
[125] J. Coraux, A.T. N'Diaye, C. Busse, T. Michely, Nano Lett. 8 (2008) 565–570.
[126] A.T. N'Diaye, J. Coraux, T.N. Plasa, C. Busse, T. Michely, New J. Phys. 10 (2008) 043033.
[127] Z.H. Zhou, F. Gao, D.W. Goodman, Surf. Sci. 604 (2010), L31-L38.
[128] Y. Xu, L. Semidey-Flecha, L. Liu, Z.H. Zhou, D.W. Goodman, Faraday Discuss. 152 (2011) 267–276.
[129] L. Liu, Z.H. Zhou, Q.L. Guo, Z. Yan, Y.X. Yao, D.W. Goodman, Surf. Sci. 605 (2011) L47–L50.
[130] C.L. Song, B. Sun, Y.-L. Wang, Y.P. Jiang, L.L. Wang, K. He, X. Chen, P. Zhang, X. C. Ma, Q.K. Xue, Phys. Rev. Lett. 108 (2012) 156803.
[131] H.H. Chen, S.H. Su, S.L. Chang, B.Y. Cheng, C.W. Chong, J.C.A. Huang, M.F. Lin, Carbon 93 (2015) 180–186.
[132] W.C. McKee, M.C. Patterson, J.R. Frick, P.T. Sprunger, Y. Xu, Catal. Today 280 (2017) 220–231.
[133] A. Goriachko, Y.B. He, H. Over, J. Phys. Chem. C 112 (2008) 8147–8152.
[134] A. Goriachko, Y.B. He, M. Knapp, H. Over, M. Corso, T. Brugger, S. Berner, J. Osterwalder, T. Greber, Langmuir 23 (2007) 2928–2931.
[135] M.C. Patterson, B.F. Habenicht, R.L. Kurtz, L. Liu, Y. Xu, P.T. Sprunger, Phys. Rev. B 89 (2014) 205423.
[136] Y. Han, A.K. Engstfeld, R.J. Behm, J.W. Evans, J. Chem. Phys. 138 (2013) 134703.
[137] J.V. Barth, G. Costantini, K. Kern, Nature 437 (2005) 671–679.
[138] W. Yang, X. Lu, G. Chen, S. Wu, G. Xie, M. Cheng, D. Wang, R. Yang, D. Shi, K. Watanabe, T. Taniguchi, C. Voisin, B. Plaçais, Y. Zhang, G. Zhang, Nano Lett. 16 (2016) 2387–2392.
[139] P.Y. Huang, C.S. Ruiz-Vargas, A.M. van der Zande, W.S. Whitney, M.P. Levendorf, J.W. Kevek, S. Garg, J.S. Alden, C.J. Hustedt, Y. Zhu, J. Park, P.L. McEuen, D.A. Muller, Nature 469 (2011) 389–392.
[140] K. Kim, Z. Lee, W. Regan, C. Kisielowski, M.F. Crommie, A. Zettl, ACS Nano 5 (2011) 2142–2146.
[141] F. Varchon, P. Mallet, J.-Y. Veuillen, L. Magaud, Phys. Rev. B 77 (2008) 235412.
[142] E. Loginova, S. Nie, K. Thurmer, N.C. Bartelt, K.F. McCarty, Phys. Rev. B 80 (2009) 085430.
[143] D.W. Kim, Y.H. Kim, H.S. Jeong, H.T. Jung, Nat. Nanotechnol. 7 (2012) 29–34.
[144] J.H. Son, S.J. Baeck, M.H. Park, J.B. Lee, C.W. Yang, J.K. Song, W.C. Zin, J.H. Ahn, Nat. Commun. 5 (2014) 3484.
[145] D.W. Kim, J.M. Ok, W.B. Jung, J.S. Kim, S.J. Kim, H.O. Choi, Y.H. Kim, H.T. Jung, Nano Lett. 15 (2015) 229–234.
[146] M.A. Shehzad, S. Hussain, J. Lee, J. Jung, N. Lee, G. Kim, Y. Seo, Nano Lett. 17 (2017) 1474–1481.
[147] D.L. Duong, G.H. Han, S.M. Lee, F. Gunes, E.S. Kim, S.T. Kim, H. Kim, Q.H. Ta, K. P. So, S.J. Yoon, S.J. Chae, Y.W. Jo, M.H. Park, S.H. Chae, S.C. Lim, J.Y. Choi, Y.H. Lee, Nature 490 (2012) 235–239.

Please cite this article in press as: J. Yang et al., Self-organized growth and self-assembly of nanostructures on 2D materials, FlatChem (2017), http://dx.doi.org/10.1016/j.flatc.2017.07.004